

AD-A058 905

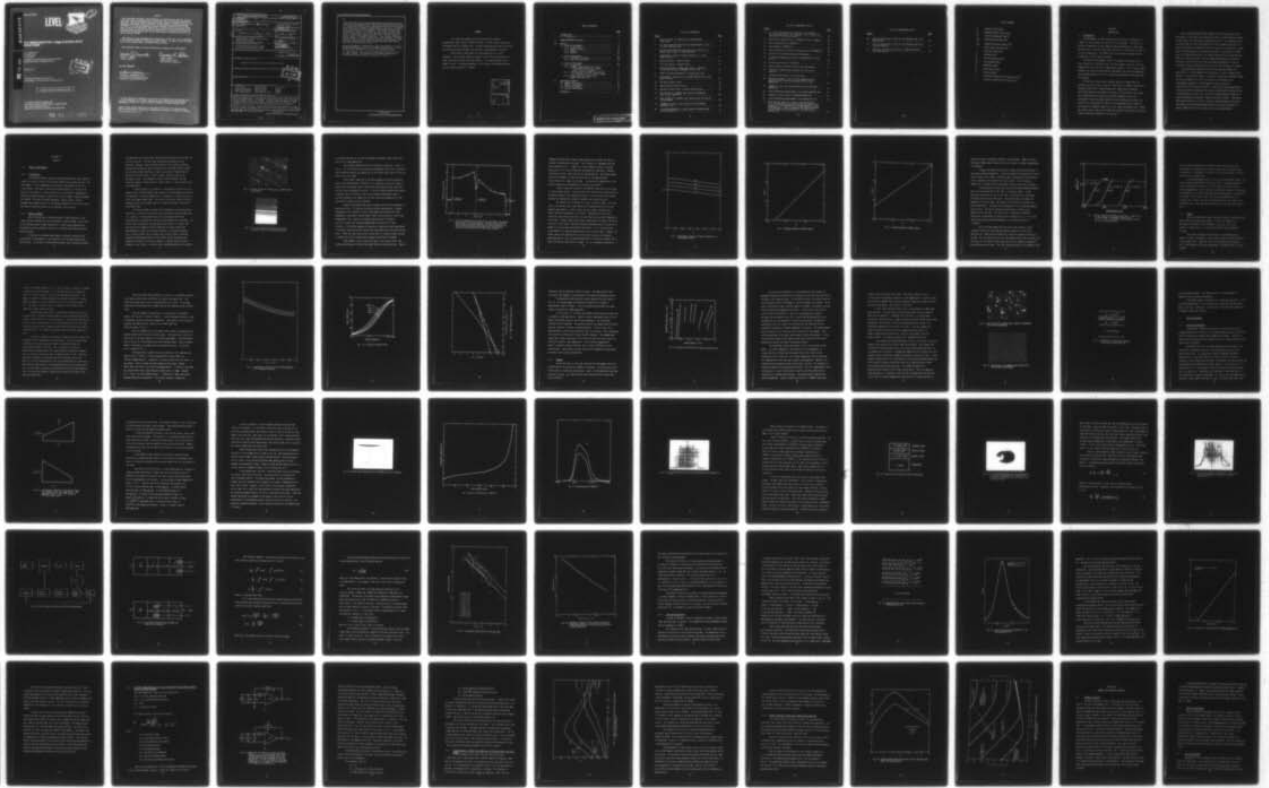
ROCKWELL INTERNATIONAL THOUSAND OAKS CALIF SCIENCE --ETC F/G 17/5  
III-V SEMICONDUCTOR 1.06 MICROMETERS ELECTRO-OPTIC STRUCTURES.(U)

UNCLASSIFIED

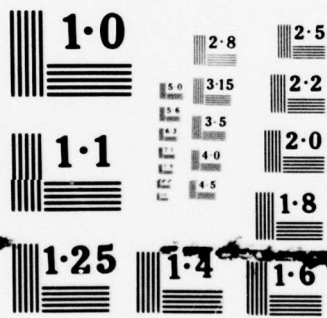
MAR 78 L R TOMASETTA, H D LAW, J S HARRIS  
SC5086.14TR AFAL-TR-78-34

F33615-77-C-1005  
NL

1 OF 1  
ADA  
058905



END  
DATE  
FILMED  
11-78  
DDC



NATIONAL BUREAU OF STANDARDS

AFAL-TR-78-34

**LEVEL III**



AD A058905

**III-V SEMICONDUCTOR 1.06 $\mu$ m ELECTRO-OPTIC STRUCTURES**

L. R. TOMASETTA  
H. DAVID LAW  
J. S. HARRIS

ROCKWELL INTERNATIONAL SCIENCE CENTER  
THOUSAND OAKS, CALIFORNIA 91360

MARCH 1978

TECHNICAL REPORT AFAL-TR-78-34  
Interim Report - October 20, 1976 - October 20, 1977



DDC FILE COPY

Approved for public release; distribution unlimited.

AIR FORCE AVIONICS LABORATORY  
AIR FORCE WRIGHT AERONAUTICAL LABORATORIES  
AIR FORCE SYSTEMS COMMAND  
WRIGHT-PATTERSON AIR FORCE BASE, OHIO 45433

78 09 11 072

NOTICE

When Government drawings, specifications, or other data are used for any purpose other than in connection with a definitely related Government procurement operation, the United States Government thereby incurs no responsibility nor any obligation whatsoever; and the fact that the government may have formulated, furnished, or in any way supplied the said drawings, specifications, or other data, is not to be regarded by implication or otherwise as in any manner licensing the holder or any other person or corporation, or conveying any rights or permission to manufacture, use, or sell any patented invention that may in any way be related thereto.

This report has been reviewed by the Information Office (OI) and is releasable to the National Technical Information Service (NTIS). At NTIS, it will be available to the general public, including foreign nations.

This technical report has been reviewed and is approved for publication.

Donald J. Peacock

DONALD J. PEACOCK  
Project Engineer

Donald R. Locker

DONALD LOCKER  
Acting Group Leader  
Electro-Optic Detectors

FOR THE COMMANDER

William C. Schoonover

WILLIAM C. SCHOONOVER, Chief  
Electro-Optics Technology Branch  
Electronic Technology Division

"If your address has changed, if you wish to be removed from our mailing list, or if the addressee is no longer employed by your organization please notify AFAL/DHO-3, W-PAFB, OH 45433 to help us maintain a current mailing list".

Copies of this report should not be returned unless return is required by security considerations, contractual obligations, or notice on a specific document.

⑨ Interim technical rept. 20 Oct 76 - 20 Oct 77

SECURITY CLASSIFICATION OF THIS PAGE (When Data Entered)

19 REPORT DOCUMENTATION PAGE		READ INSTRUCTIONS BEFORE COMPLETING FORM													
1. REPORT NUMBER 8 AFAL TR-78-34	2. GOVT ACCESSION NO.	3. RECIPIENT'S CATALOG NUMBER													
4. TITLE (and Subtitle) III-V SEMICONDUCTOR 1.06 <sup>micrometers</sup> ELECTRO-OPTIC STRUCTURES.		5. TYPE OF REPORT & PERIOD COVERED Technical Report - Interim 10/20/76--10/20/77													
7. AUTHOR(s) 10 L. R. Tomasetta, H. David/Law, J. S. Harris		6. PERFORMING ORG. REPORT NUMBER 44 SC5086.14TR													
9. PERFORMING ORGANIZATION NAME AND ADDRESS Science Center, Rockwell International 1049 Camino Does Rios Thousand Oaks, California 91360		8. CONTRACT OR GRANT NUMBER(s) 15 F33615-77-C-1005 <i>new</i>													
11. CONTROLLING OFFICE NAME AND ADDRESS Air Force Avionics Laboratory (DHO) Wright-Patterson AFB, Ohio 45433		10. PROGRAM ELEMENT, PROJECT, TASK AREA & WORK UNIT NUMBERS 16 2907 03-67 17 03													
14. MONITORING AGENCY NAME & ADDRESS (if different from Controlling Office) 6 2504F		12. REPORT DATE 17 March 1978													
16. DISTRIBUTION STATEMENT (of this Report) Approved for public release; distribution unlimited.		13. NUMBER OF PAGES 74													
17. DISTRIBUTION STATEMENT (of the abstract entered in Block 20, if different from Report)		15. SECURITY CLASS. (of this report) UNCLASSIFIED 12 84e													
18. SUPPLEMENTARY NOTES		15a. DECLASSIFICATION/DOWNGRADING SCHEDULE													
19. KEY WORDS (Continue on reverse side if necessary and identify by block number)															
<table border="0"> <tr> <td>1.06 microns</td> <td>Laser Receiver</td> <td>III-V Alloy</td> </tr> <tr> <td>Liquid Phase Epitaxy</td> <td>GaAs FET Preamp</td> <td>GaAsSb</td> </tr> <tr> <td>Avalanche Photodiode</td> <td>Heterojunction</td> <td>GaAlSb</td> </tr> <tr> <td>Laser Communication</td> <td>Light Emitting Diode</td> <td>InGaAsP</td> </tr> </table>				1.06 microns	Laser Receiver	III-V Alloy	Liquid Phase Epitaxy	GaAs FET Preamp	GaAsSb	Avalanche Photodiode	Heterojunction	GaAlSb	Laser Communication	Light Emitting Diode	InGaAsP
1.06 microns	Laser Receiver	III-V Alloy													
Liquid Phase Epitaxy	GaAs FET Preamp	GaAsSb													
Avalanche Photodiode	Heterojunction	GaAlSb													
Laser Communication	Light Emitting Diode	InGaAsP													
20. ABSTRACT (Continue on reverse side if necessary and identify by block number)															
<p>The most significant results to date have been concentrated in the material and device development area. In the material area, three alloys systems have been explored, GaAsSb, GaAlSb, and InGaAsP. The high dislocation density of GaAsSb has been reduced by a series of lattice matching layers. An intensive study of dopants in this material has been made and doping control to the low <math>10^{15} \text{ cm}^{-3}</math> has been achieved. A doping drop method has been developed to reduce interface defects and compositional variation in the grown layer. In the GaAlSb</p>															

DDC  
SEP 19 1978  
F

DD FORM 1 JAN 73 1473 EDITION OF 1 NOV 65 IS OBSOLETE

Unclassified

SECURITY CLASSIFICATION OF THIS PAGE (When Data Entered)

16 to the 15th power per cm cm.  
389 949

JCB

20.

system the better lattice match between epilayer and substrate results in a very smooth surface morphology. Avalanche photodiodes fabricated from this system show extremely uniform photoresponse over the entire optically active area even at microwave avalanche gains as high as 20. A detailed study of the electron and hole ionization coefficients have been made and indicate a factor of two difference. This implies an excess multiplication noise factor of 0.75 which, although larger than the silicon (0.4), is significantly smaller than GaAs (1.0). The most promising material system is the InGaAsP quaternary. In this system, the epilayer lattice constant is "forced" to match that of the substrate. The best surfaces of any III-V system have been achieved in the quaternary. LEDs fabricated from grown layers show excellent performance, and lifetime tests are currently being initiated.

Avalanche photodetector improvement has been concentrated in the area of improved photoresponse uniformity at moderate avalanche gains. In the GaAlSb system, high speed ( $t_r < 80$  ps), high quantum efficiency ( $\eta > 80\%$ ), detectors with uniform microwave avalanche gains of 16-20 have been achieved. These diodes have the highest speed-quantum efficiency performance reported for any APDs at  $1.06 \mu\text{m}$ .

Unclassified

## FORWORD

This report was prepared by the Science Center, Rockwell International under Contract F33615-77-C-1005. This work covers the period 20 October 1976 to 20 October 1977. The work described herein was carried out by the Science Center, Rockwell International, Thousand Oaks, California.

The principal investigator for the project was Dr. Louis R. Tomasetta. The principal technical support for this work was provided by H. David Law, Kenichi Nakano and Richard Gelatt. The program manager was Dr. James S. Harris. The program manager for this project from Wright-Patterson Air Force Base was Donald J. Peacock.

ACCESSION for	
NTIS	White Section <input checked="" type="checkbox"/>
DDC	Buff Section <input type="checkbox"/>
UNANNOUNCED	<input type="checkbox"/>
JUSTIFICATION	
BY	
DISTRIBUTION/AVAILABILITY CODES	
	SPECIAL
A	

## TABLE OF CONTENTS

	<u>Page</u>
I. INTRODUCTION .....	1
1.1 Introduction.....	1
II. PROGRAM APPROACH AND GOALS.....	3
III. RESULTS.....	5
3.1 Material Development.....	5
3.1.1 Introduction.....	5
3.1.2 GaAsSb, GaAlAsSb.....	5
3.1.3 GaAlSb.....	16
3.1.4 InGaAsP.....	24
3.2 Device Development.....	30
3.2.1 Avalanche Photodiodes.....	30
3.2.2 Light Emitting Diodes.....	53
3.3 Receiver Development.....	60
3.3.1 Introduction.....	60
3.3.2 DC-5MHz 1.06 $\mu$ m Receiver for Laser- Illuminated Airborn Night Imaging "Laser Line Scan" Systems.....	62
3.3.3 5 MHz Bandwidth, 100 MHz Tuned Receiver for Airborne "Laser Line Scan" Systems.....	65
3.3.4 Gigabit Data-Rate 1.06 $\mu$ m Laser Communication Receiver.....	68
IV. CONTINUING RESEARCH.....	71
4.1 Summary of Results.....	71
4.2 Material Development.....	72
4.3 Device Development.....	72
4.4 Receiver Development.....	73
REFERENCES.....	74

## LIST OF ILLUSTRATIONS

<u>Figure</u>		<u>Page</u>
1	Typical Surface of a GaAs <sub>0.95</sub> Sb <sub>0.15</sub> Showing Rough Cross Hatch.....	7
2	A 7 Layer Structure APD Grown From GaAsSb Material, With 4 Lattice Matching Layer.....	7
3	Sb Profile Obtained From X-Ray Emission on SEM for Two GaAsSb Layers Grown on a GaAs Substrate.....	9
4	Experimental Liquidus of GaAsSb, Measured in a Transparent Furnace.....	11
5	Germanium Doping in GaAsSb System.....	12
6	Tellurium Doping in GaAsSb System.....	13
7	Optical Absorption of GaAs <sub>1-x</sub> Sb <sub>x</sub> Alloys. Shown Also is the Mole Percent and Bandgap of Each Alloy.....	15
8	Typical Surface Morphology of a Ga <sub>0.55</sub> Al <sub>0.45</sub> Sb Layer.....	17
9	Experimental Liquidus Curve of GaAlSb Measured by a Transparent Furnace.....	21
10	Solidus of GaAlSb Alloys.....	22
11	Band Diagram of GaAlSb Alloys.....	23
12	Absorption Coefficients of Several GaAlSb Alloys.....	25
13	Bad Surface of a InGaAsP Layer Caused by Phosphorous Loss at High Temperature.....	28
14	Good Surface of an InGaAsP Layer Grown by the InP Cap and In bath Method.....	28
15	Schematic of a Four Layer Structure Lattice Matched InGaAsP/InP LED.....	29
16	A Low Noise APD Design, a Read Structure Prevents Mixed Carrier Generation.....	32

LIST OF ILLUSTRATIONS (Cont'd)

<u>Figure</u>	<u>Page</u>
17 a). A Flat Electrified Profile Diode., This Structure Will Have Lower Noise. b). Contrary to Fig. 3.17(a), This Structure Will Have Higher Noise.....	33
18 Reverse Bias Characteristics of F9B2S2-F3, 20 mil Diameter...	36
19 Gain vs Reverse Bias of F9B2S2-F3.....	37
20 Photoresponse of F9B2S2-F3.....	38
21 Scan Cross-section of the Gain Characteristics of F9B2S2-F3..	39
22 Structure of the GaAlSb Avalanche Photodiodes.....	41
23 An Intensity Modulated Scan Over the F10B1S1-G5 at a Gain of 10.....	42
24 A Scan Cross-section of F10B1S1-G5.....	44
25 Block Diagram of Ionization Coefficients Measurement.....	47
26 Structure of GaAlSb Diodes Suitable for Pure Carrier Injection.....	43
27 Ionization Coefficients for Ga <sub>0.74</sub> Al <sub>0.26</sub> Sb.....	51
28 Breakdown Voltages of the Uniformly Doped One-sided Abrupt Junction n-type Ga <sub>0.74</sub> Al <sub>0.26</sub> Sb Diodes at Room Temperature.....	52
29 Schematic of Six Layer Double Heterostructure GaAlAsSb/GaAsSb LED.....	55
30 Electroluminescence Measurement of the GaAlAsSb/GaAsSb LED...	56
31 Intensity vs Bias Current of GaAlAsSb/GaAsSb LED.....	58
32 Electroluminescence Measurement of the InGaAsP/InP LED.....	59
33 Model Used for Analysis of Signal and Noise Response. e <sub>1</sub> is the Equivalent Input Noise Voltage Generator of the Preamp, e <sub>2</sub> is the Johnson Noise Voltage Generator of the Conductance G <sub>f</sub> . In(b), G <sub>I</sub> Replaces the Input Conductance of the Preamp and the Conductance of the APD and i <sub>nj</sub> Replaces e <sub>2</sub> .....	63

LIST OF ILLUSTRATIONS (Cont'd)

<u>Figure</u>		<u>Page</u>
34	Signal to Noise Ratio vs Gain for the Baseband Laser Line Scan Receiver.....	66
35	Signal to Noise Ratio vs Gain for the 100 MHz Tuned Laser Line Scan Receiver.....	69
36	Comparison of Alternative Detector Preamp Combinations for 1 GB/s Receiver.....	70

## LIST OF SYMBOLS

$E$	Electric Field (V/cm)
$E_m$	Maximum Electric Field (V/cm)
$\Delta f$	Electrical Bandwidth ( $\text{sec}^{-1}$ )
$i_{nj}^2$	Johnson Noise Current ( $A^2$ )
$i_{ne}^2$	Preamplifier Noise Current ( $A^2$ )
$\ell$	Active Layer Thickness ( $\mu\text{m}$ )
$L$	Diffusion Length ( $\mu\text{m}$ )
$M$	Avalanche Gain
$M_n$	Electron Avalanche Gain
$M_p$	Hole Avalanche Gain
$m$	Modulation Index
$X_n$	Excess Noise Factor
$W$	Depletion Width
$\alpha$	Ionization Coefficient for Electrons ( $\text{cm}^{-1}$ )
$\beta$	Ionization Coefficient for Holes ( $\text{cm}^{-1}$ )

## SECTION I

### INTRODUCTION

#### 1.1 Introduction

The development of higher performance electro-optical components at  $1.06\mu\text{m}$  is vital to present and future Air Force Programs. Two devices of particular importance are the  $1.06\mu\text{m}$  avalanche photodiode and  $1.06\mu\text{m}$  light emitting diode. Two areas where these devices are of particular interest to Air Force programs are (1) Nd:YAG laser active imaging and communication systems and (2) Fiber optical systems.

The materials development currently in progress will extend the Air Forces capability in airborne laser line scan systems, high data rate laser communication, and fiber optic communication systems. For all three of these systems, very significant performance improvements over existing technology has been demonstrated for the III-V avalanche photodetectors developed under this program.

The materials being studied, GaAsSb, GaAlSb and InGaAsP have the potential not only to meet current Air Force needs at  $1.06\mu\text{m}$  by replacing Si avalanche diodes and S-1 photocathodes which cannot meet the quantum efficiency-bandwidth requirements of current Air Force efforts, but because their energy gap can be adjusted by different component ratios, the development of high technology growth and device processing of these alloy materials will provide the Air Force with a technology base to extend its electro-optical component capability to even longer wavelengths (e.g.  $1.27\mu\text{m}$ ) where fiber optical cables with higher data capability and superior radiation hardness have been developed in the last year.

The avalanche photodiode (APD) program has been directed toward the development of high speed, high quantum efficiency avalanche detectors, mated to high speed, low noise hybrid integrated receivers. This approach and the resulting superior receiver performance has clearly demonstrated that it is absolutely essential to develop the optical receiver as a coherent unit rather than as separate detector and electronics efforts. The comparison of APDs grown for  $1.06\mu\text{m}$  applications in the three different alloy systems described above will provide assurance that the  $1.06\mu\text{m}$  photodetectors and receivers delivered to the Air Force will have the highest performance in terms of quantum efficiency, bandwidth and noise that current technology can produce.

These performance parameters are of prime importance whether the application is a 5 MHz baseband line scan system, a 1 GBit/s communication system or a fiber optical system. In addition to the high performance  $1.06\mu\text{m}$  receiver development, this III-V alloy materials technology can be advantageously applied to the development of novel sources for state-of-the-art fiber optical systems. Fiber optical systems operating at  $1.06\mu\text{m}$  have superior performance over current system based on GaAlAs devices at  $0.82\mu\text{m}$  because of lower fiber loss due to reduced Rayleigh scattering at longer wavelengths and because of improved radiation hardness. High speed, superradiant operation of LED will provide a high performance source which when mated with the high performance detectors previously described will produce communication links far superior to any yet demonstrated.

## SECTION II

### PROGRAM APPROACH AND GOALS

The 1.06 $\mu$ m Electro-Optic Structures Program consists of three projects: avalanche photodiodes, optical receivers and LED fiber optical sources.

The goal of the avalanche photodiodes project is to fabricate high quantum efficiency ( $>95\%$ ), high speed ( $t_r < 50ps$ ), uniform gain ( $15 < M < 30$ ), low bulk leakage avalanche photodiodes in three material systems: GaAsSb, GaAlSb and InGaAsP. With high quality diodes fabricated from each material fundamental studies of the hole and electron ionization rates and the excess noise factor can be made. The best material choice for a given system application can then be made.

The double heterostructure photodiode approach used successfully in previous contract work in the GaAsSb system will be applied to the GaAlSb and InGaAsP systems. Refinements in epilayer growth techniques and doping control will extend the performance of the GaAsSb devices to include not only high quantum efficiency but also high uniform gain. The same refinements combined with our experience in GaAs and GaAsSb diodes will quickly permit the development of high quantum efficiency GaAlSb and InGaAsP APDs.

In order to take advantage of the high speed of the APDs described above, the preamplifier which follows the APD must have high speed, with the lowest possible equivalent input noise. This preamplifier, when combined with an APD becomes a high speed, high sensitivity optical receiver.

Our approach to develop improved optical receivers is based on the hybrid integration of the APD with the other semiconductor devices that

comprise the preamplifier. The value of this technique has been demonstrated in previous optical receiver contract work. The basic transimpedance feedback amplifier design permits the optical receiver to take full advantage of the extremely low input capacitance of the APD and GaAs FET technology available at the Science Center by allowing larger feedback resistance values and therefore lower Johnson or thermal noise than possible with other amplifier designs or higher capacitance devices. The integration of all components in chip form on a single substrate reduces stray capacitance effects which, because of the extremely low capacitance associated with the APD ( $<.2\text{pf}$ ) and GaAs FET ( $<.3\text{pf}$ ), could easily be the dominate total capacitance.

The goal of the LED project is to produce high efficiency, ultimately superradiant, high speed devices suitable for coupling into single fiber cables. Lifetimes of 5,000-10,000 hours are necessary for reliable system applications.

Our approach will be directed at fabricating double heterostructures using GaAsSb or InGaAsP. Techniques will be developed for growing very thin ( $< 0.5\mu\text{m}$ ) active layers with carefully lattice matched confining layers. Reducing lattice mismatch defects at the confining layer boundary is vital to achieve long lifetime devices. High efficiency will be achieved by fabricating superradiant device geometries. By amplifying the radiation traveling in the plane of the junction, and reflecting it into a fiber, order of magnitude increases in power should be possible.

Finally, the power coupled into an optical fiber will be measured. It is the improvement in power coupled into a fiber that is of prime concern for fiber communication systems.

## SECTION III

### RESULTS

#### 3.1 Material Development

##### 3.1.1 Introduction

The high performance 1.06 $\mu$ m avalanche photodiodes and light emitting diodes to be used in the Air Force Gigabit Communication System and Laser Line Scan Imager is vitally dependent on the material development of the III-V alloy systems. Previously, reported device performance was limited by the quality of the material. During the past year, considerable improvement of materials has been achieved in several III-V alloy systems; GaAlSb, GaAlAsSb and InGaAsP. The material growth parameters, doping studies, lattice parameter measurements as well as the bandgap composition variation of each of the materials mentioned above will be reported in this section.

##### 3.1.2 GaAsSb, GaAlAsSb

One of the problems of growing GaAsSb on a GaAs substrate is the large difference between the lattice constants of GaAs and GaSb. The strains of the epilayers grown on GaAs substrate will likely cause degradation of performance or even catastrophic failures in avalanche photodiodes and light emitting diodes.

In the case of avalanche photodiodes, the defects (caused by the dislocations in the GaAsSb) will be responsible for the high recombination dark current. In the case of light emitting diodes, these dislocation defects

are responsible for the dark spots which grow with time and finally cause the failure of the LED. In either case, the dislocation defects are not desirable. Moreover, these dislocation defects can be greatly reduced by growing lattice matching layers. Epilayers with increasing antimony content can be grown on GaAs substrates to lower the dislocation induced etch pit density of the active layer. Figure 1 shows a typical surface of the GaAs<sub>0.85</sub>Sb<sub>0.15</sub> layer. The roughness is due to lattice mismatch, and the lines are aligned in <100> direction. Figure 2 shows a 7 layer structure with 5 matching layers.

In early growth of this material, a considerable variation in alloy composition was observed between layers grown at the same temperature and from the same melts. The alloy composition,  $X$ , increased (i.e. greater Sb in the solid) with higher growth rates. This effect could be due either to lattice constant pulling at low growth rates or to arsenic depletion in the melt at high growth rates.

At the slow growth rate under near thermodynamic equilibrium growth conditions, a lattice pulling effect shifts the equilibrium point toward GaAs (i.e. lower  $X$ ). At high growth rates, the melt becomes sufficiently supersaturated to overcome this lattice pulling tendency and  $X$  increases. The possibility of As depletion at high growth rates results in a higher than equilibrium solid composition due to depletion of arsenic because the replenishment of arsenic at the growth interface is limited by diffusion. Thus, at higher growth rates, a higher mole fraction of GaSb is obtained. Determining unequivocally which of these effects causes the growth rate composition variation is difficult; however, it appears that the arsenic depletion is more likely. In earlier work on GaAsSb photodiodes, we observed

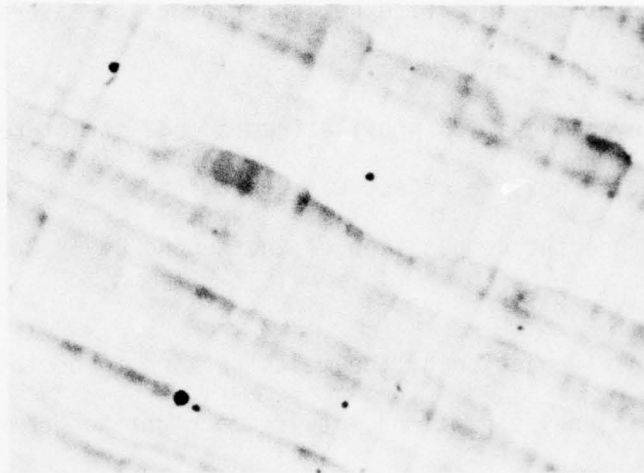


Fig. 1 Typical Surface Of A  $\text{GaAs}_{.95}\text{Sb}_{.15}$  Showing Rough Cross-Hatch.

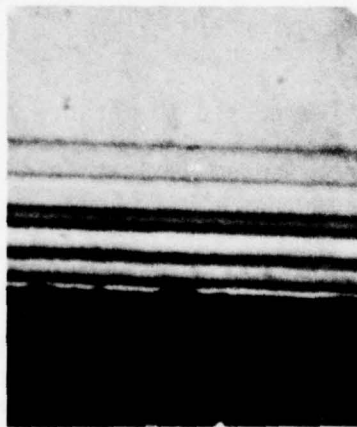


Fig. 2 A 7 Layer Structure APD Grown From GaAsSb Material, With 4 Lattice Matching Layer.

an antimony decrease at the interface between two GaAsSb layers grown from melts of the same composition.

The antimony composition profile from such a structure is shown in Fig. 3. If the lattice pulling effect was predominant, then such a dip would not be observed because the composition of the second layer would be pulled to that of the first layer.

Since arsenic depletion of the melts appears to be the predominant cause of the compositional variations, it is important to grow all layers at sufficiently low growth rates to achieve near equilibrium growth conditions and thus assure reproducible results. A series of GaAsSb growths were made at a cooling rate of  $0.75^{\circ}\text{C}/\text{min}$ . and lattice constant measurements made to precisely determine the composition so that the desired composition in the multilayer structure could be achieved.

Gandolfi measurements were used to measure the lattice parameters as described earlier. In addition to precise lattice determination, an added advantage of this technique is that a semi-quantitative measure of layer homogeneity is obtained from the width of the x-ray diffraction lines on the photographic film. Growth at a furnace cooling rate of  $0.75^{\circ}\text{C}/\text{min}$ . results in layers with constant compositions as a function of layer thickness. The solidus composition observed in these more recent experiments is different from our earlier results with high growth rates and rapid cooling rates. These new "near equilibrium" solidus data is currently being utilized to improve our earlier ternary phase diagram calculations for GaAsSb.

There appears to be a miscibility gap in this ternary alloy. One cannot grow epilayers with more than 20% of GaSb on a GaAs substrate. Several

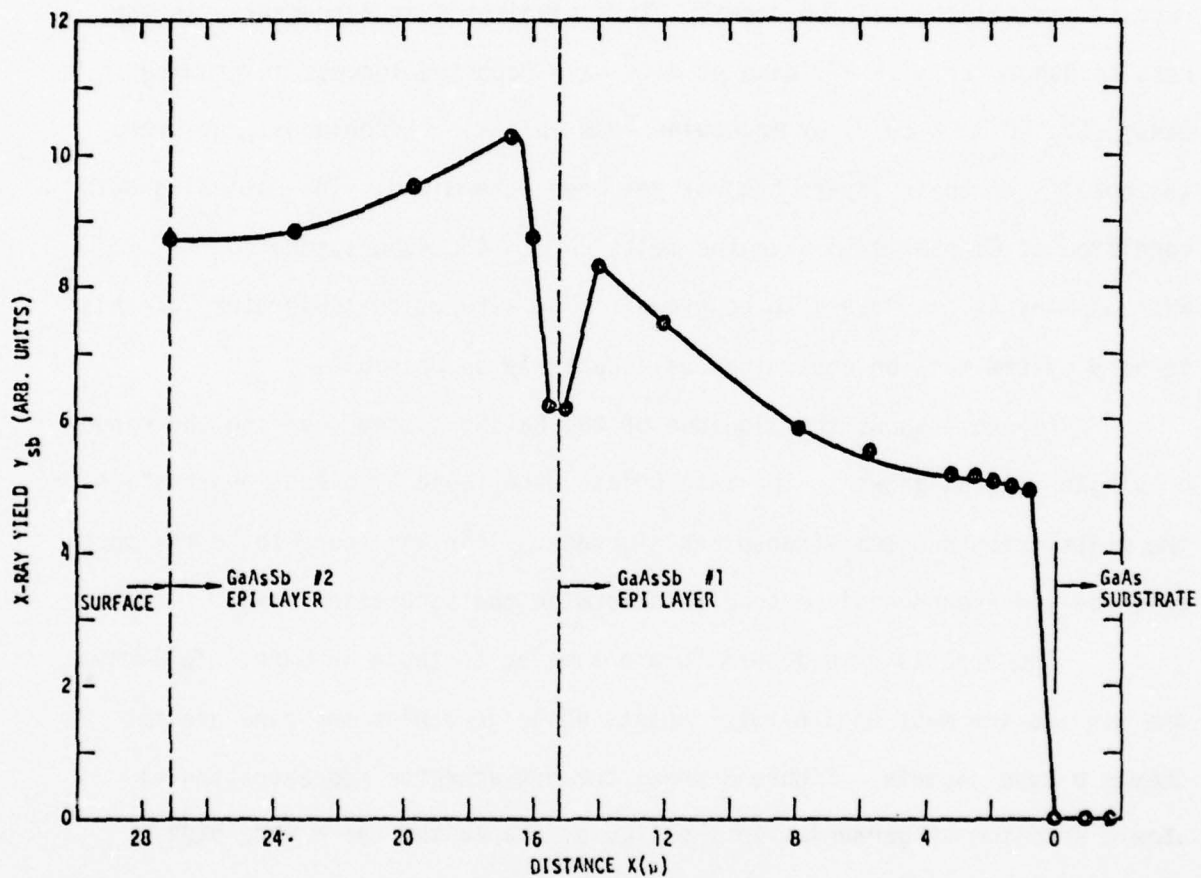


Fig. 3 Sb Profile Obtained From X-Ray Emission On SEM For Two GaAsSb Layers Grown On A GaAs Substrate. The Melt Composition For Each Epitaxial Layer Was Identical But Growth Conditions, At The Time The Second Melt Was Brought Over The Substrate, Caused The Sb Concentration To Dip At The Interface.

attempts have been made to grow a GaAs<sub>0.78</sub>Sb<sub>0.22</sub> alloy on GaAs, but they all resulted in polycrystalline growth. This finding is in agreement with the results Nahory et al.<sup>1</sup> T. Waho et al.<sup>2</sup> have reported success in growing GaAs<sub>1-x</sub>Sb<sub>x</sub> (0.3 < x < 0.9) by molecular beam epitaxial techniques. However, the quality of their layers has not yet been determined. The optimal growth condition of GaAsSb is to have the melts 2°C to 4°C supersaturated with as many as six layers to be grown. The saturation temperature of this ternary system must be determined as accurately as possible.

Figure 4 shows the liquidus of the GaAsSb system covering the range of single crystal growth. The data points were found by direct observation of the melts through a semi-transparent furnace. This was found to be the most accurate and reproducible method to determine the saturation point.

The dopants used in GaAsSb are similar to those in GaAs. Tellurium and tin are the most used n-type dopants while germanium and zinc are the common p-type dopants. Figure 5 shows the net acceptor concentration vs atomic fraction of germanium in the liquid. Germanium has a very high solubility in gallium and normally will not affect the saturation temperature of the melt. Figure 6 shows the net donor concentration vs atomic fraction of tellurium in the liquid. The most noticeable characteristics of tellurium in GaAsSb is its very high distribution coefficient. It is a very desirable n-type dopant for a heavily doped contact layer or buffer layer. However, for better control and reproducibility of the active layer of the avalanche photodiode where a very low doping concentration is required, a dopant with a lower distribution coefficient is needed. Tin is a reasonable alternative. A

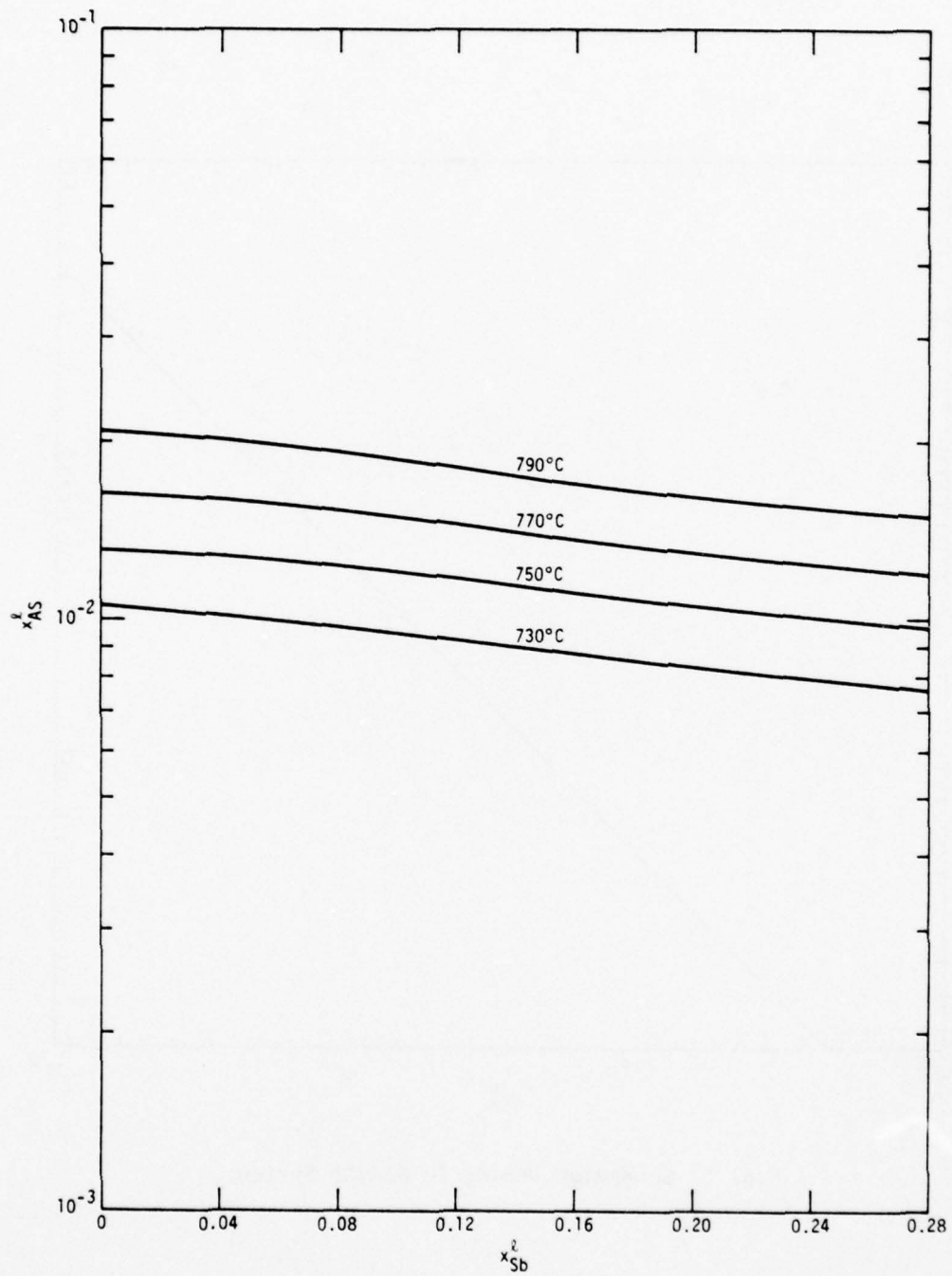


Fig. 4 Experimental Liquidus Of GaAsSb, Measured In A Transparent Furnace.

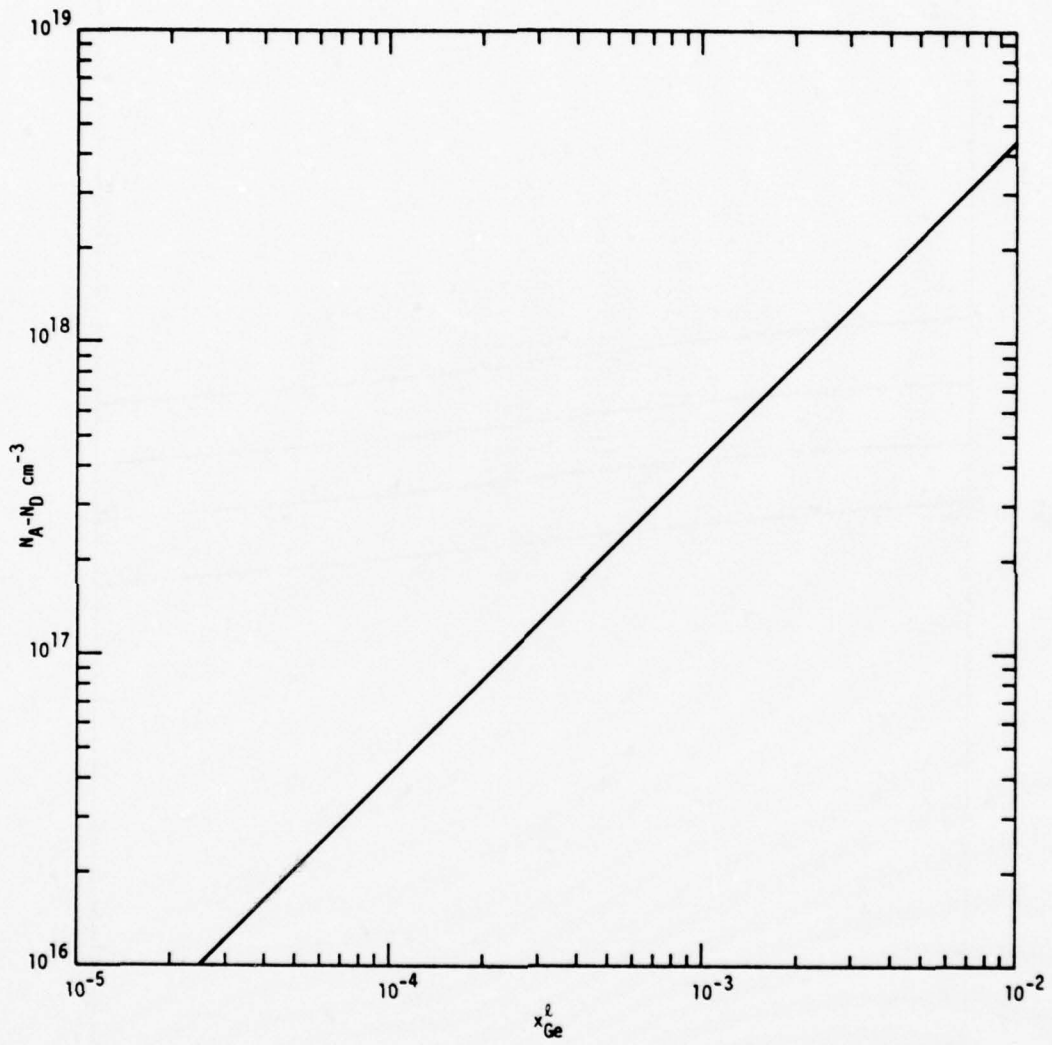


Fig. 5 Germanium Doping In GaAsSb System.

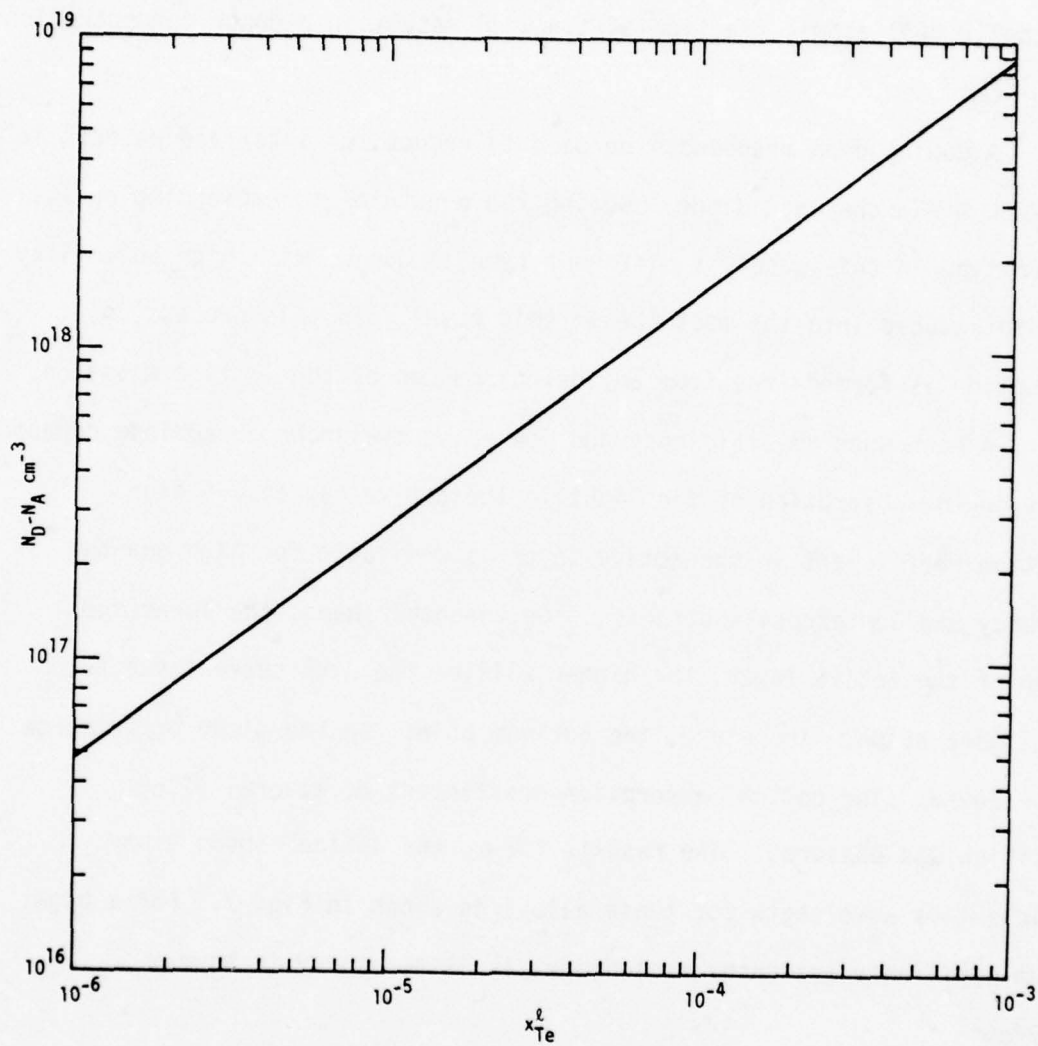


Fig. 6 Tellurium Doping In GaAsSb System.

detailed study of tin doping in GaAsSb is not available. However, we have found that 0.0001 atomic fraction of tin will result in a donor concentration of  $3 \times 10^{15} \text{cm}^{-3}$ .

A doping drop method can be used to reduce the interface defects in the GaAsSb avalanche photodiode. During the growth of the absorbing or active layer (n-type in this case), a different type of dopant with high solubility can be introduced into the melt (Ge in this case). In this process, a homojunction is formed free from any defect caused by the lattice mismatch.

A high quantum efficiency and low noise avalanche photodiode depends heavily on the absorption of the light in the active region. A high absorption coefficient in the active layer is desirable for high quantum efficiency and low excess shot noise. On the other hand, the lower the bandgap of the active layer, the higher will be the dark current due to thermal generation. Therefore, the optimum point for the diode performance must be found. The optical absorption coefficient of several alloy composition was measured. The results for  $\alpha$ , the optical absorption coefficient vs wavelength for these alloys is shown in Fig. 7. For a high quantum efficiency avalanche photodiode, it is necessary to have  $\alpha > 5 \times 10^3 \text{cm}^{-1}$ .

Due to the requirement that the active layer requires a high absorption coefficient the immediate matching layers will have finite absorption at  $1.06 \mu\text{m}$  and thus dramatically reduce the quantum efficiency of the APD. One can always grow the last two matching layers with less GaSb such that they will not absorb  $1.06 \mu\text{m}$  light, but this will defeat the purpose of growing the matching layers. The final interface defects really depend on the

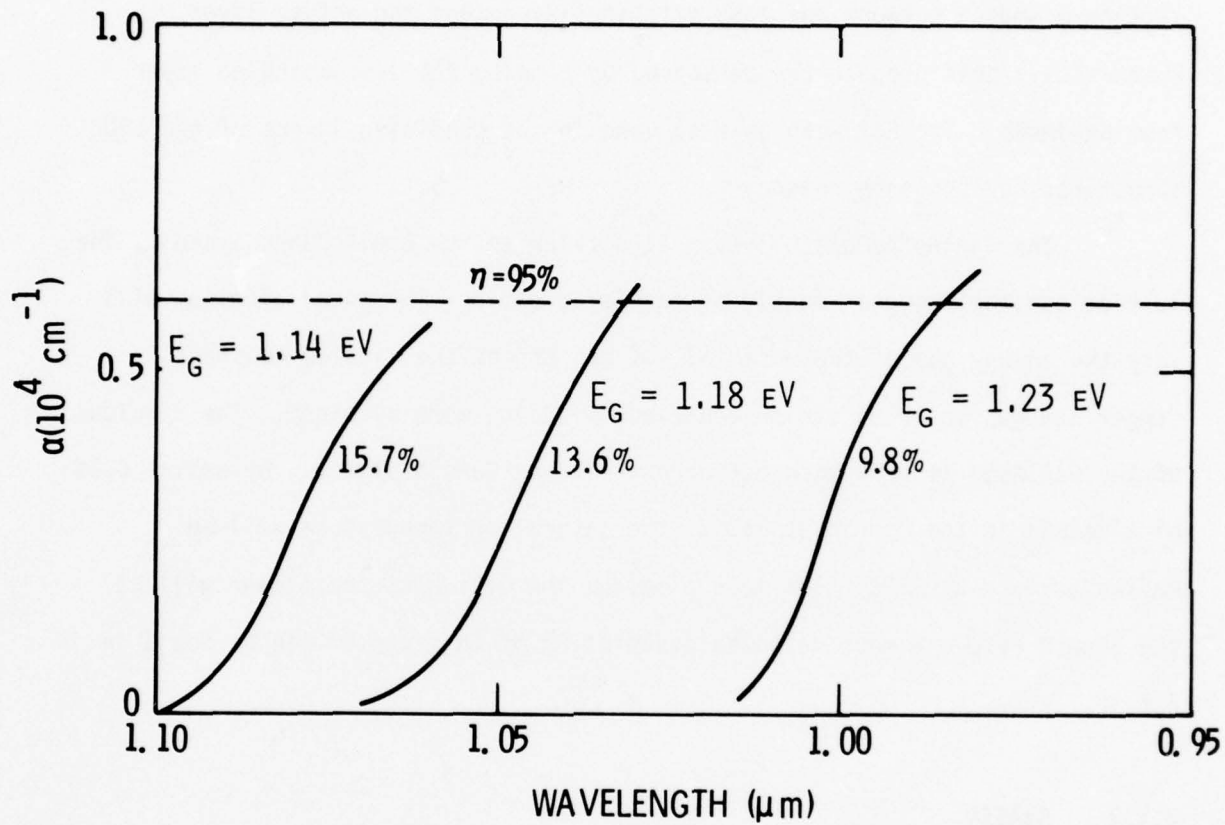


Fig. 7 Optical Absorption Of GaAs<sub>1-x</sub>Sb<sub>x</sub> Alloys. Shown Also Is The Mole Percent And Bandgap Of Each Alloy.  $\alpha = 0.6 \times 10^4 \text{ cm}^{-1}$  Results In 95% Quantum Efficiency With A  $5 \mu\text{m}$  Depletion Region.

lattice mismatch between the last matching layers and the active layer. Fortunately, this problem can be solved by growing the last matching layer from GaAlAsSb. The GaAlAsSb is also used in the confining layers of the LED structures for the same reason.

The GaAlAsSb/GaAsSb system is similar to the GaAlAs/GaAs system. The lattice constant depends mostly on the As/Sb ratio. The added aluminum will vary the energy gap of the material but not effect the lattice constant. Larger bandgap material can be achieved by adding more aluminum. The liquidus of the GaAlAsSb is very much different from the GaAsSb system. By adding 0.1% of aluminum in the liquid at 750<sup>0</sup>C, the saturation temperature will be raised as much as 25<sup>0</sup>C. The more aluminum the melt has, the slower will be the growth rate. A more detailed description of this system can be found in Ref. 3.

### 3.1.3 GaAlSb

Unlike the GaAsSb/GaAs system, the growth of GaAlSb on GaSb substrate should have a fairly good lattice match. For the full range of x in Ga<sub>1-x</sub>Al<sub>x</sub>Sb, the largest lattice mismatch is only 0.7%. For all the devices of interest here, x < 0.5 which limited the lattice mismatch to < 0.35%.

The surface morphology of the epilayer in the GaAlSb system is superior to that of the GaAsSb. Figure 8 shows a typical surface as grown of a Ga<sub>0.55</sub>Al<sub>0.45</sub>Sb layer. Comparing Fig. 8 with the GaAsSb surface shown in Fig. 1, the superiority of surface morphology in the GaAlSb layer is clearly evident.



Fig. 8 Typical Surface Morphology Of A  $\text{Ga}_{.55}\text{Al}_{.45}\text{Sb}$  Layer.

One of the key elements of achieving good epitaxial growth is the surface preparation and removal of surface oxides immediately prior to growth. The substrate polishing in GaSb is not straightforward since the surface of the substrate is extremely sensitive to every step in polishing process prior to growth. Several methods work well in polishing the GaSb substrates. A carbosyl + H<sub>2</sub>O<sub>2</sub> + H<sub>2</sub>O polish on cloth after 3 $\mu$ m alumina grit lapping provides a mirror surface. However, this method leaves quite a large amount of mechanical damage which shows up under a 3% Br-CH<sub>3</sub>OH etch. A better method which minimizes the polishing damage has been developed. A solution consisting of 1cc bromine, 800cc of methanol and 200cc of glycerol is used to polish the GaSb on a rotating disc. A higher percentage of bromine can be used at first to polish the substrate down to one mil greater than the desired thickness. Then, the above solution is used as the final polish. The 0.1% bromine solution was found to be the optimum solution. A higher percentage of bromine results in faster chemical etching action during polish and usually leaves rounded edges on the substrate. On the other hand, a lower percentage of bromine in the solution reduces the chemical etching and cause more mechanical damage on the substrate surface. The glycerol in the solution plays the role of an inert lubricant. A complex oxide, which is difficult to dissolve, can easily form on the polished surface of the GaSb substrates. This makes the sample preparation procedure prior to growth very critical. In order to get a good growth, these complexes must be prevented from forming during every wafer cleaning procedure. The polished substrate is boiled in trichloroethylene, acetone, methanol and isopropyl alcohol in that order. At

no time is the sample exposed to air. After cleaning in solvents, the sample is blown dry by clean nitrogen. It is then put into HF for 5 minutes to remove all residual oxides. The HF is then quenched with methanol. The sample is etched in 2% bromine-methanol with constant agitation. A large amount of methanol is used to quench the etch so as to prevent exposure to air. The sample is finally rinsed in isopropyl alcohol, blown dry and immediately loaded into the furnace.

An equivalently good result is obtained by stripping the surface of the substrate by an anodic oxidation method. The polished GaSb substrate is solvent cleaned, and then is oxidized anodically. A low current density must be used in the oxidation process or the polished substrate will turn rough. The grown oxides are then stripped by concentrated HF solution and rinsed in isopropyl alcohol. This method considerably reduces substrate preparation time.

A second key element in the growth of GaAlSb is precise control over the degree of melt supersaturation during growth. In order to obtain good nucleation and resulting epitaxial growth, the GaAlSb melt must be supersaturated between 2° and 4°C. This is especially critical for GaAlSb because at approximately 5°C supersaturation, polycrystal formation occurs in the bulk of the melt and all supersaturation is lost. The quick polycrystal formation is associated with the fast growth rate of this material. With no supersaturation, the ternary GaAlSb melt will etch back a GaSb substrate and very poor surface morphology and layer uniformity result. Thus, in multi-layer structures, each melt must be precisely equilibrated so that it has the exact degree of supersaturation required for growth at the substrate temperature.

Since the growth rate of GaAlSb is so fast, it is essential to have a slow furnace cooling rate ( $<0.2^{\circ}\text{C}/\text{min}$ ) to control the growth rate. The slower the growth rate, the less stacking faults will result. It has been experimentally determined that a slower cooling rate produces better epitaxial layers.

Since the degree of supercooling is so important to the GaAlSb growth, the liquidus is studied in detail. A semi-transparent furnace is used to determine the exact saturation temperature. Data points of this study are observed near  $500^{\circ}\text{C}$  and the liquidus line at  $490^{\circ}$ ,  $500^{\circ}$  and  $510^{\circ}\text{C}$  are shown in Fig. 9.

The solid composition of the GaAlSb layers cannot be measured by the Gandolfi method due to the close lattice match. The resolution of the x-ray diffraction is not good enough for an accurate measurement. The percentage of AlSb in the solid is best measured by the microprobe method. Once a standard sample is available, the composition can be measured easily. The solidus curve is shown in Fig. 10.

The energy band of GaAlSb alloys was studied in this laboratory by Anderson et al.<sup>4</sup> GaSb is a direct bandgap material while AlSb is an indirect bandgap material. Therefore, a crossover should occur for some  $x$  in  $\text{Ga}_{1-x}\text{Al}_x\text{Sb}$ . Figure 11 shows the band diagram of  $\text{Ga}_{1-x}\text{Al}_x\text{Sb}$ . Beyond 18% of AlSb, the alloy is an indirect bandgap material. It does not seem that  $\text{Ga}_{1-x}\text{Al}_x\text{Sb}$  should have a high absorption coefficient at  $1.06\mu\text{m}$ . However, for  $x = 0.26$ ,  $\Gamma$  is just  $0.028\text{ eV}$  above  $L$ . Therefore at  $1.06\mu\text{m}$ , the direct bandgap dominates the absorption. This effect, moreover, reduces the

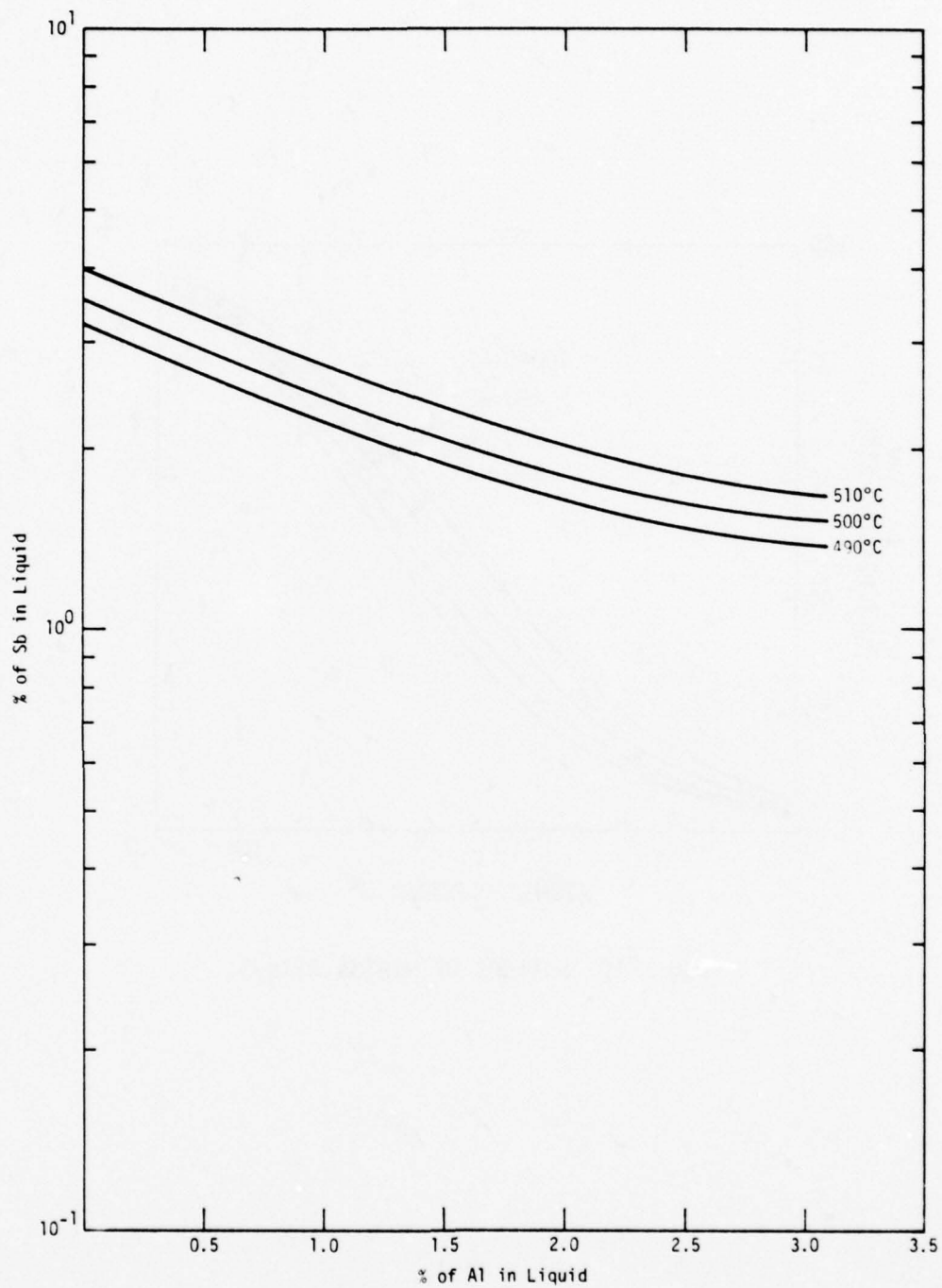


Fig. 9 Experimental Liquidus Curve Of GaAlSb Measured By a Transparent Furnace.

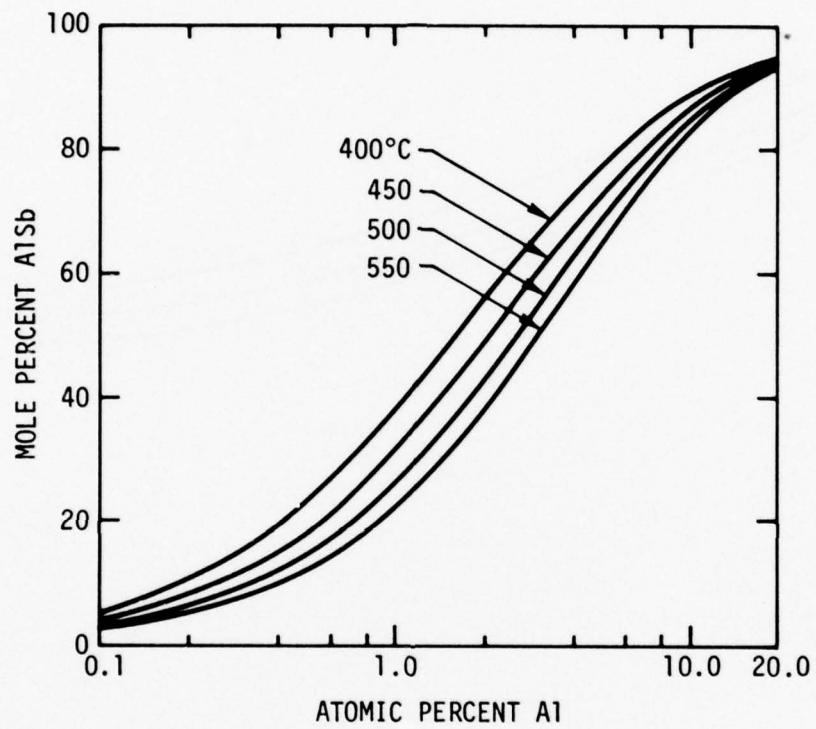


Fig. 10 Solidus Of GaAlSb Alloys.

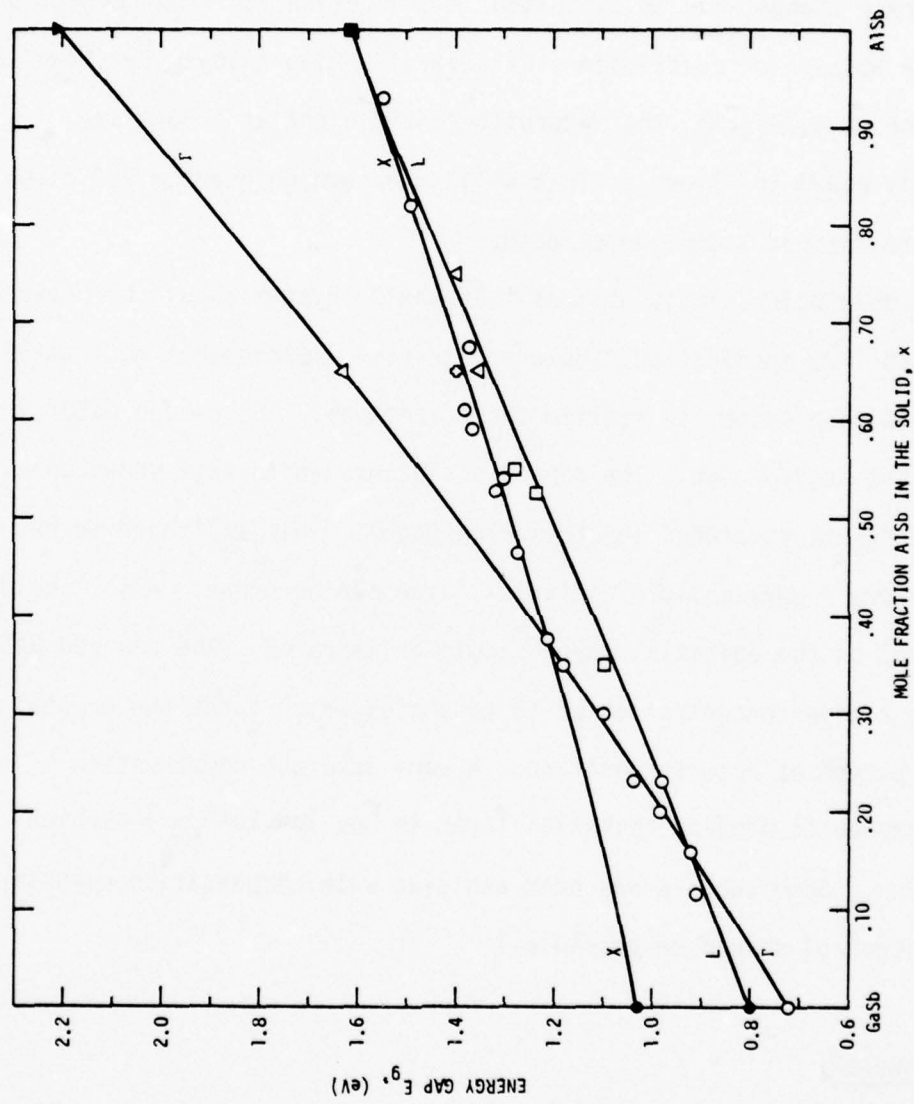


Fig. 11 Band Diagram of GaAlSb Alloys.

ionization rate of electrons relative to holes. The implication of this ionization rate change will be discussed in the Device Performance section.

The absorption coefficients of several GaAlSb alloys are shown in Fig. 12. For  $\text{Ga}_{0.74}\text{Al}_{0.26}\text{Sb}$ , the absorption coefficient at  $1.06\mu\text{m}$  is approximately equal to  $10^4\text{cm}^{-1}$ . This will produce high quantum efficiency diodes at the desired  $1.06\mu\text{m}$  wavelength.

At this point, it is obvious that GaAlSb system should be better than the GaAsSb for APD application. However, several improvements must still be made on the GaAlSb system to realize the advantages. The n-type GaSb substrate must be improved. The doping striations and damage shows up clearly when the substrate is etched in Bromine-methanol. This will have to be improved before a more uniform epitaxial layer can be grown. Also, the doping level control on the epitaxial layer should be improved. The undoped GaSb layers have a high concentration of Sb vacancies which turns the crystal to  $1 \times 10^{17}\text{cm}^{-3}$  p-type at room temperature. A very accurate compensation dopant is needed to produce epitaxial layer in the low  $10^{15}\text{cm}^{-3}$  carrier concentration. Some success has been achieved with compensation experiments but better control should be possible.

#### 3.1.4 InGaAsP

In the later part of last year, the material development effort has concentrated on the quarternary InGaAsP alloy system. The preliminary result of the growth is exceedingly encouraging. Layers of InP/InGaAsP/InP have been successfully grown. The light emitting diodes made from these layers were quite successful.

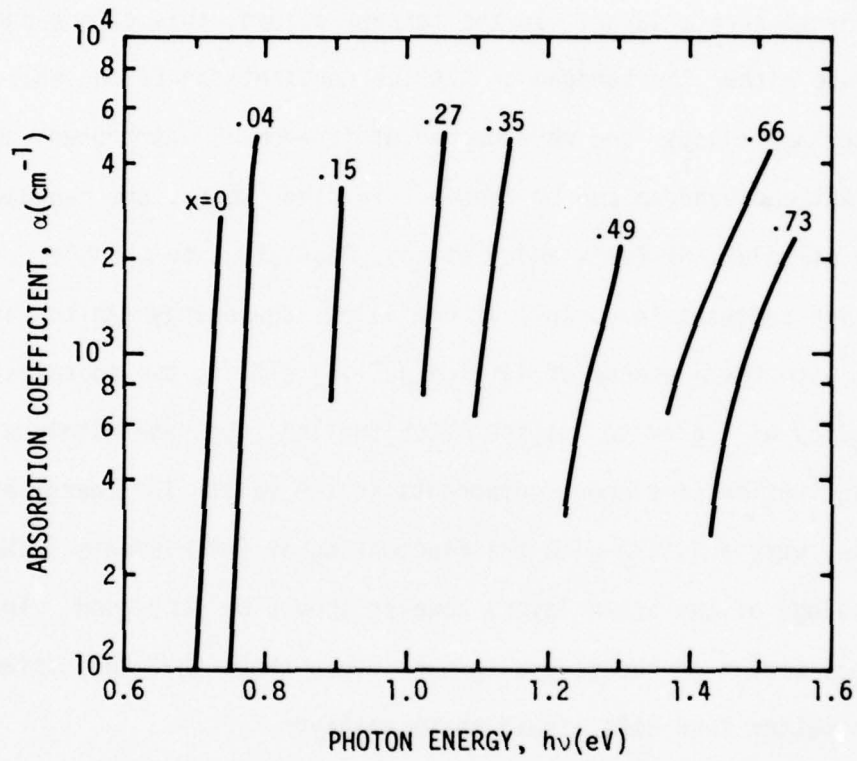


Fig. 12 Absorption Coefficients Of Several GaAlSb Alloys.

The lattice pulling effect in liquid phase epitaxial growth is a phenomenon whereby the epilayer has the tendency to grow with the same lattice constant as the substrate layer. In the ternary alloys, this effect cannot be utilized because either the bandgap or lattice constant can be chosen. In the case of quaternary alloys, one more degree of freedom is introduced, and both lattice constant and bandgap can be chosen. In other words, one can have infinite sets of solutions for  $x$  and  $y$  in  $\text{In}_{1-x}\text{Ga}_x\text{As}_y\text{P}_{1-y}$  to produce the same lattice constant (e.g. InP) if one allows the energy gap to vary. Consequently, with the presence of lattice pulling effect, the epitaxial quaternary alloy will grow to lattice match the InP substrate within a reasonable fluctuation of element components in the melt. The energy bandgap may, of course, vary a little with the fluctuation of the elements. The surface morphology of the grown layers however should be very good. In fact, the preliminary result of the several grown layers shows that the surface morphology is better than GaAs liquid phase epilayer.

The quaternary layers were grown in an In rich solution at near  $620^\circ\text{C}$ . At a lower temperature, the solubility of the phosphorous in indium solution is limited and the growth rate of InP as well as the quaternary alloy is very low. At a higher temperature, the InP substrate will degrade due to the high vapor pressure of phosphorous. However, this problem can be overcome by using a InP cap and a In bath. The substrate is covered by another InP substrate before growth. The first compartment of the sliding boat is a pure In melt which is used to etch the surface of the substrate for 5 seconds before growth. This method greatly improves the surface morphology. Figure 13 shows the surface of a InGaAsP layer grown

without using the InP cap and In bath. The surface shows a lot of In inclusion due to phosphorous vacancies at high temperatures. Figure 14 shows the surface of InGaAsP layer using the same melt composition grown by the InP cap and In wash method. The surface is excellent.

A four layer structure shown in Fig. 15 was grown for 1.06 $\mu$ m light emitting diode. A buffer layer of InP was grown from a melt saturated at 625 $^{\circ}$ C and was doped to  $n = 3 \times 10^{18} \text{cm}^{-3}$  with tellurium. A lattice match quaternary layer emitting at 1.06 $\mu$ m is grown from a melt consisting of 0.33% phosphorous, 1% of arsenic, 0.17% of gallium dissolved in indium. The saturation temperature of this melt is at 611 $^{\circ}$ C. The solid composition grown from this melt turns out to be In<sub>0.89</sub>Ga<sub>0.11</sub>As<sub>0.25</sub>P<sub>0.75</sub>, and it is doped to  $2 \times 10^{17} \text{cm}^{-3}$  with tellurium. Finally, a InP contact layer was grown at 603 $^{\circ}$ C. This layer was doped to  $p = 3 \times 10^{18} \text{cm}^{-3}$  with zinc.

The relatively wide spectrum shown in Fig. 32 is possibly a result of compositional grading of the active layer during growth. The standard LPE technique of cooling the melt (6 $^{\circ}$ C in this case) during growth was used. As the temperature of the melt is changed the composition of the grown solid also changes slightly resulting in composition grading in the active layer. In the GaAsSb and GaAlSb there is no alternative to cooling during growth because the melts typically cannot tolerate more than 2 $^{\circ}$ C of supersaturation without precipitating polycrystalline growth. The InGaAsP system can be supersaturated as much as 10 $^{\circ}$ C without precipitation. With this degree of supersaturation it is possible to equilibrate the temperature and grow the active layer at constant temperature using the built-in supersaturation to

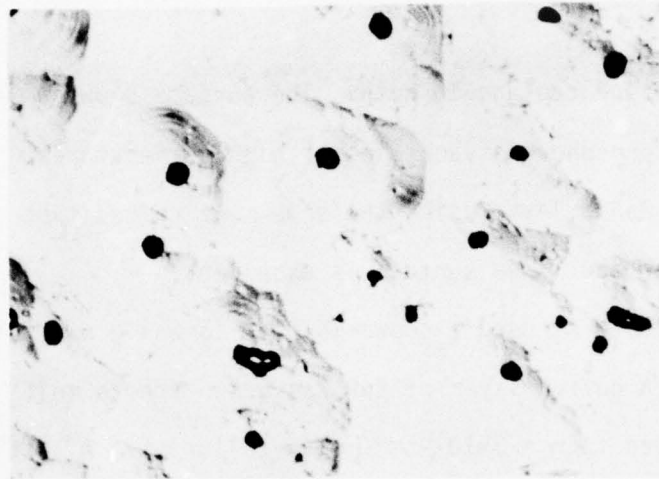


Fig. 13 Bad Surface Of A InGaAsP Layer Caused By Phosphorous Loss At High Temperature.

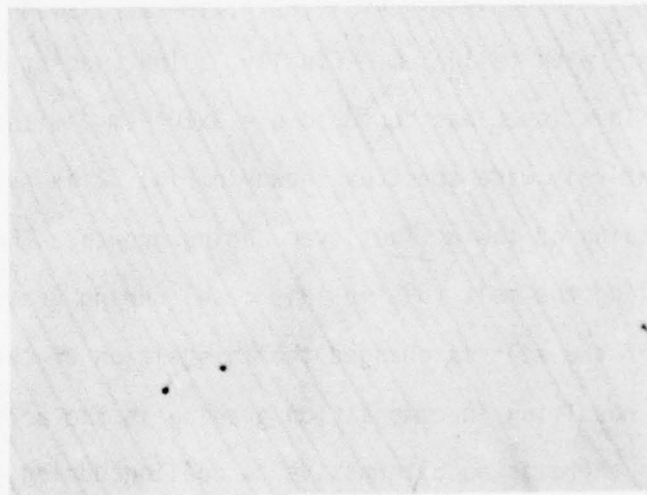


Fig. 14 Good Surface Of A InGaAsP Layer Grown By The InP Cap And In Bath Method.

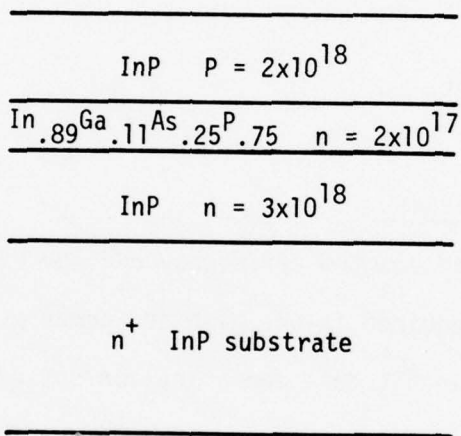


Fig. 15 Schematic Of A Four Layer Structure Lattice Match InGaAsP/InP LED.

drive the growth process. This should result in a constant material composition and a narrower LED spectrum.

A good ohmic contact is essential to a light emitting diode. In the preliminary measurement, it does not seem that a good ohmic contact can be made on InP layer. Eventually, a fourth layer of lattice match InGaAsP will be needed for good ohmic contact.

### 3.2 Device Development

#### 3.2.1 Avalanche Photodiodes

A high speed, high quantum efficiency and low excess shot noise avalanche photodiode is required in the high performance optical receiver for laser line scanning and gigabit data communication systems. In order to achieve both high speed and high quantum efficiency, a double heterostructure device must be employed.

The excess noise of an avalanche photodiode can be assumed to be proportional to  $M \exp(X_n)$ ; where  $M$  is the avalanche gain and  $X_n$  is the excess noise factor.  $X_n$  is basically a material dependent parameter. Theoretically, if the ionization rate of one kind of carrier (holes or electrons) is much larger than the other, the secondary ionization process can be considered to be caused by one carrier species. In this case,  $X_n = 0$ . Contrary to this, if the ionization rates of electrons and holes are equal,  $X_n$  will be equal to 1. Therefore, the anisotropy of ionization rates is very important for detector performance. In silicon, the ionization rate for electrons is much higher than that for holes. An excess noise factor ( $X_n$ )

equal to 0.4 is observed. By careful design of the diode, a  $X_n$  of 0.3 can be achieved. The Read structure diode as shown in Fig. 16 is such a design. The avalanche field is on the right hand side of the diode, while the absorption region is on the left. In this structure, the primary carriers (electron in this case) are created in the low field region. When they enter the avalanche zone, only a small number of holes exist so the primary carriers are basically one type. Therefore, it has the lowest excess noise. This structure can be implemented easily in silicon. In order to achieve the almost flat field in the absorption region, a very low doping is necessary. Carrier concentrations lower than  $10^{15}\text{cm}^{-3}$  in III-V alloy system are very difficult to achieve. Consequently, the absorption region and the avalanche region in III-V alloy diodes cannot be as easily separated as in silicon. As a result, most III-V avalanche photodiodes have the problem of mixed carrier generation which increases the excess shot noise. Knowing that the secondary ionization process depends on the integral of the electric field in the region of carrier travel, one can choose the structure as in Fig. 17(a) rather than the one in Fig. 17(b). In Fig. 17(a), most of the primary carriers are absorbed in the lower field region, thus the secondary carrier feedback effect is less than that in the structure shown in Fig. 17(b). In Fig. 17(b) the excess shot noise will be larger because of the poorer statistical distribution caused by the secondary carrier feedback.

The speed of a photodiode depends on the capacitance of the diode as well as the transit time of the carriers through the diode. Lowering the doping of the active region will increase the depletion region and therefore reduce the capacitance of the diode. Increasing the depletion width, however,

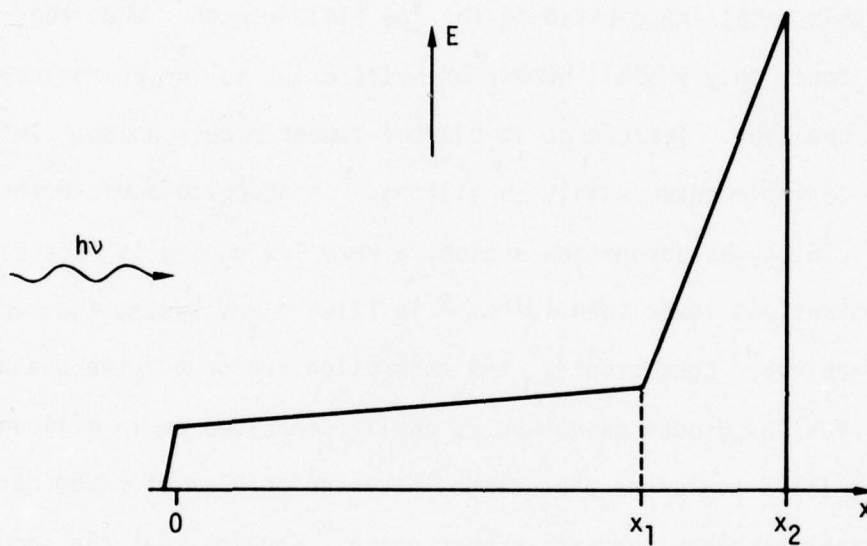
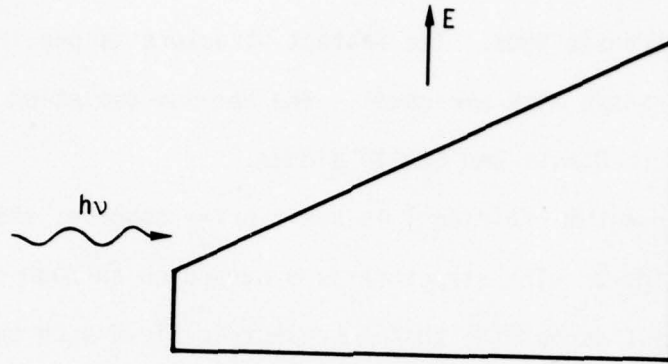
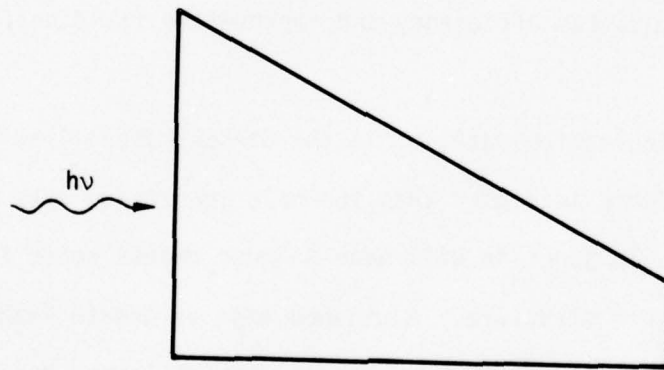


Fig. 16 A Low Noise APD Design, The Read Structure Prevents Mixed Carrier Generation. The Absorption And Drift Region Is From  $0-x$ , And The Avalanche Zone Is From  $x_1-x_2$ .



(a)



(b)

Fig. 17 (a) Electric Field For A Flat Profile Diode. This Structure Will Have Lower Noise. (b) Compared To Fig. 17 (a), This Structure Will Have Higher Noise.

increases the carrier transit time. The fastest structure is one in which the RC time constant and transit time are equal. The optimum depletion width is found to be 3-4 $\mu$ m in both GaAsSb and GaAlSb diodes.

If speed and quantum efficiency is not a prime concern, then a lower noise diode can be designed. The structure is a non-punch-through design in which absorption of light is outside the high electric field such that pure carriers are injected into the depletion region only by diffusion. However, the quantum efficiency and the speed of the diode will be seriously degraded in this structure.

In the GaAsSb system, improved, uniform gain diodes have been fabricated by growing GaAlAsSb layers, lattice matched to the GaAsSb active layer, to increase the quantum efficiency and improve the field uniformity of the diode.

The electron ionization rate,  $\alpha$ , in the GaAsSb material suitable for 1.06 $\mu$ m avalanche photodiode is higher than the hole ionization rate  $\beta$ .<sup>5</sup> Therefore, the present n<sup>+</sup>p junction will have a lower excess noise factor than one complementary p<sup>+</sup>n structure. A stained edge of growth F9B252-F3 is shown in Fig. 2. Starting from the p<sup>+</sup> substrate, the epilayers are: 1) first lattice matching layer, p<sup>+</sup> GaAs.<sub>98</sub>Sb.<sub>02</sub>; 2) second lattice matching layer, p<sup>+</sup> GaAs.<sub>95</sub>Sb.<sub>05</sub>; 3) third matching layer, p<sup>+</sup> GaAs.<sub>92</sub>Sb.<sub>08</sub>; 4) fourth lattice matching and barrier layer, p<sup>+</sup> Ga.<sub>90</sub>Al.<sub>10</sub>As.<sub>84</sub>Sb.<sub>16</sub>; 5) absorbing active layer, thickness  $\approx$  1.5 $\mu$ m, p = 1x10<sup>16</sup>cm<sup>-3</sup>, GaAs.<sub>836</sub>Sb.<sub>164</sub>; 6) absorbing active layer, n = 5x10<sup>15</sup>cm<sup>-3</sup>, GaAs.<sub>836</sub>Sb.<sub>164</sub> thickness = 4.2 $\mu$ m; 7) contact layer n<sup>+</sup> GaAs.<sub>836</sub>Sb.<sub>164</sub>.

In order to prevent a lattice mismatch problem inside the high electric field region, it is desirable to have the lattice constant of the last lattice matching layer very nearly or equal to that of the active layer. However, by doing this, some light will be absorbed in this lattice matching layer and thus, lower the quantum efficiency of the device. Therefore, 10% of aluminum was added to form a quaternary layer with the same lattice constant, but larger bandgap than the active layer.

Figure 18 shows the reverse bias characteristics of diode F9B252-F3. The gain vs bias voltage curve is shown in Fig. 19. The sloping baseline at low bias might be due to space charge widening effect.<sup>6</sup> The photoresponse curve is shown in Fig. 20 indicating that GaAs<sub>0.836</sub>Sb<sub>0.164</sub> has an energy bandgap corresponding to 1.07 $\mu$ m. Figure 21 shows the gain characteristics of a cross section of F9B252-F3 diodes, with an average gain of 8.

In the GaAsSb diode, the basic limitation seems to be the uniformity of electric field inside the diode. The nonuniformity is caused by the lattice mismatch defects. The doping drop method, in which germanium is dropped into the n-type melt during growth, can produce a homojunction with exact lattice match. However, if the electric field punches through the active layer (as it should for high quantum efficiency, high speed operation), the interface mismatch defects will occur in the high field region. Since the thermal generation rate depends on the square of the intrinsic carrier concentration in the depletion region, the dark current will be high. The purpose of doping drop method is thus offset and the gain of the GaAsSb diode is limited.

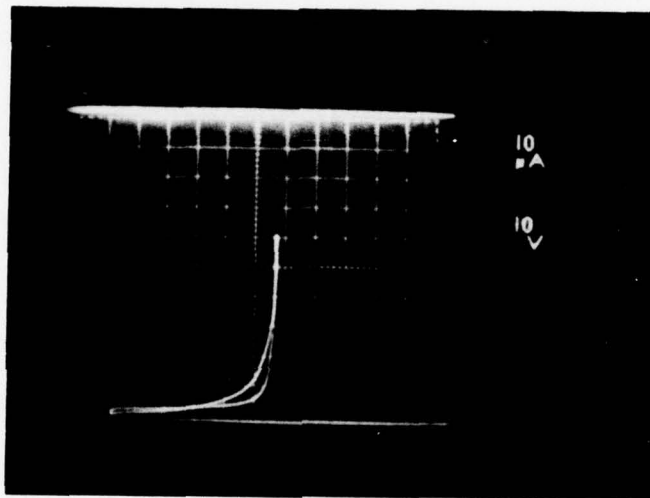


Fig. 18 Reverse Bias Characteristics Of F9B2S2-F3, 20 mil Diameter.

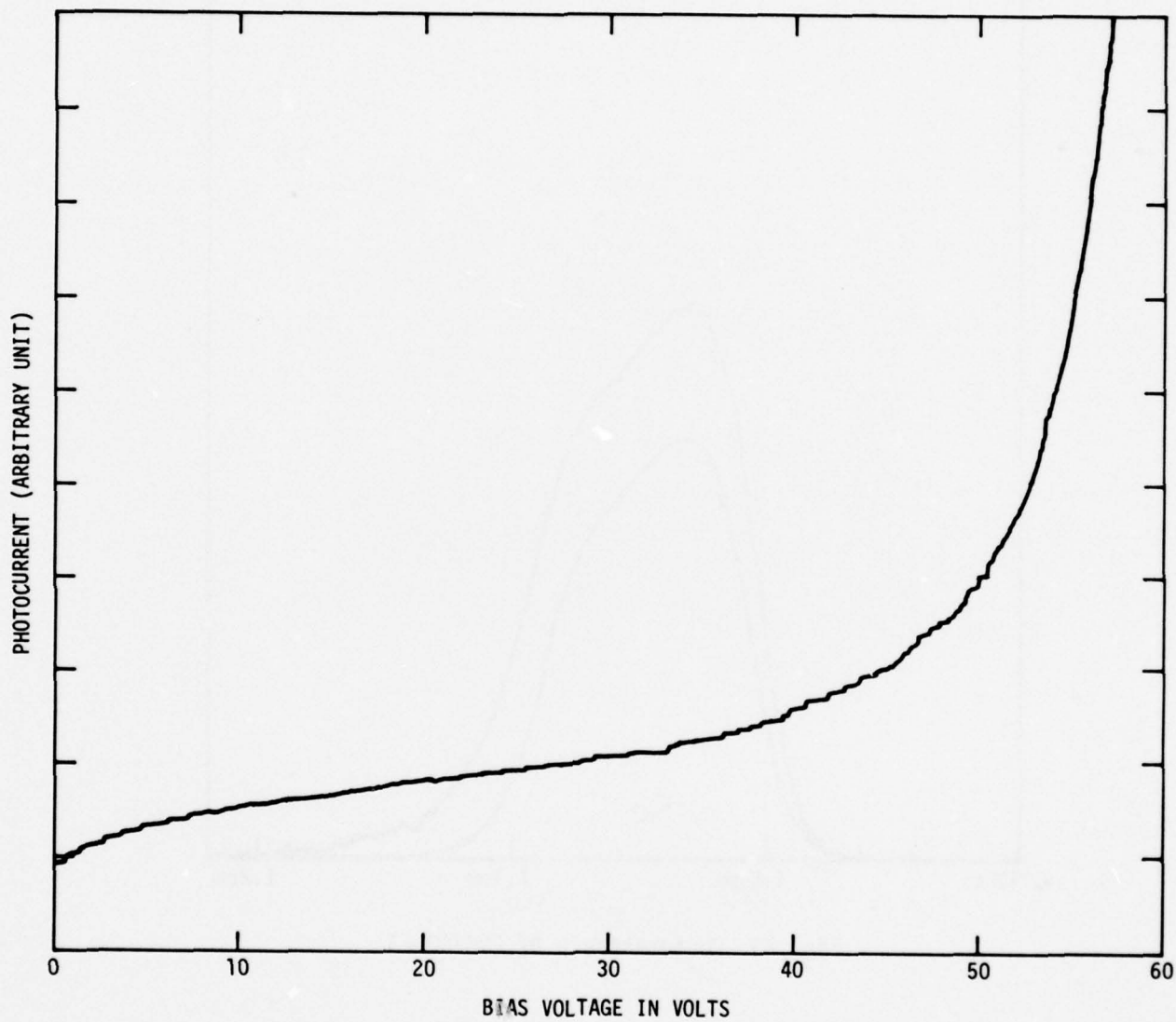


Fig. 19 Gain vs. Reverse Bias Of F9B2S2-F3.

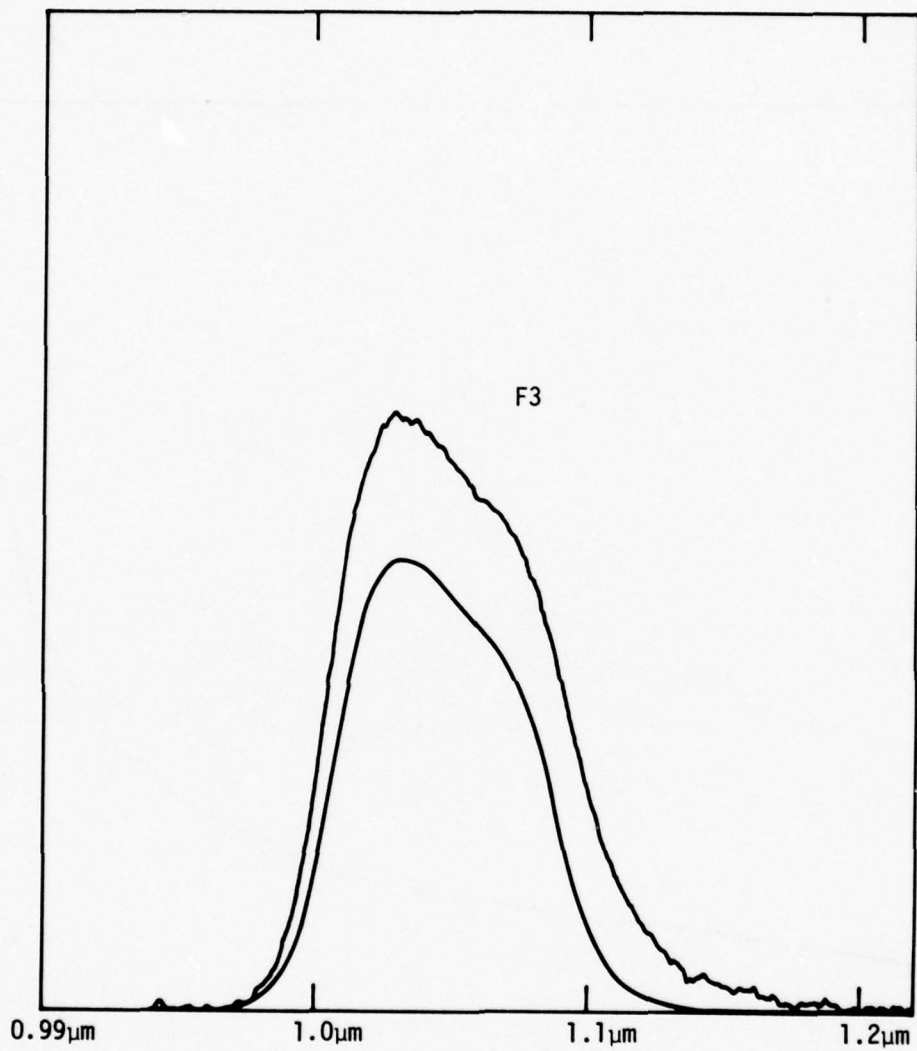


Fig. 20 Photoresponse Of F9B2S2-F3.

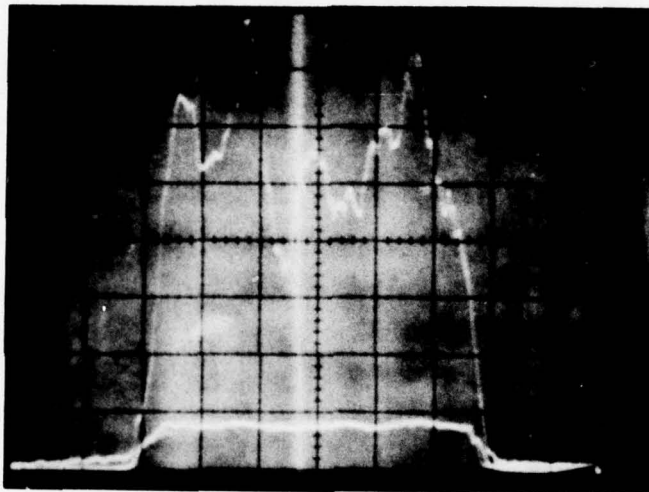


Fig. 21 Scan Cross-Section Of The Gain Characteristics Of F9B2S2-F3,  
M = 8.

Better results are obtained in the GaAlSb diodes. The GaAlSb is a fairly good lattice match system and the internal junction defects do not appear to be a major problem.

Figure 22 shows the structure of a GaAlSb avalanche photodiode. The four layer structure contains: a buffer layer of  $15.5\mu\text{m}$  of  $\text{Ga}_{.84}\text{Al}_{.16}\text{Sb}$  with a donor concentration of  $\sim 10^{17}\text{cm}^{-3}$ ; an active layer of  $10.4\mu\text{m}$  of  $\text{Ga}_{.74}\text{Al}_{.26}\text{Sb}$  with a donor concentration of  $4 \times 10^{16}\text{cm}^{-3}$ ; a confining layer of  $2.7\mu\text{m}$   $\text{p}^+$   $\text{Ga}_{.74}\text{Al}_{.26}\text{Sb}$  with an acceptor concentration of  $\sim 10^{18}\text{cm}^{-3}$ ; and finally a  $3.2\mu\text{m}$   $\text{p}^+$   $\text{Ga}_{.60}\text{Al}_{.40}\text{Sb}$  window layer with an acceptor concentration of  $p \sim 10^{18}\text{cm}^{-3}$ . The illumination on this device is through the top of this structure and the light will be absorbed in the  $\text{p}^+$   $\text{Ga}_{.74}\text{Al}_{.26}\text{Sb}$  and  $\text{n}$   $\text{Ga}_{.74}\text{Al}_{.26}\text{Sb}$  region. Mesa diodes between 10 and 25 mils were etched on this layer to form diodes for optical and electrical evaluation.

A series of measurements were carried out on these GaAlSb mesa diodes. The most significant improvement is the increase in average gain. Previously, the GaAlSb layers were grown at a cooling rate of  $2^\circ\text{C}/\text{min}$ . Since the growth rate of this material is much higher than GaAs, stacking faults will result at such a high growth rate. Therefore, furnace cooling rates of  $\frac{1}{2}^\circ\text{C}-\frac{1}{4}^\circ\text{C}/\text{min}$  were used. Diodes with higher uniform gain were made from slow growth rate materials. Also, the surface morphology is better. Figure 23 shows an intensity modulated field uniformity scan of a F10B151-G5 diode. The bias is at 18.1 V and the gain is approximately 18. The uniform intensity indicates a very good junction. To measure the field uniformity

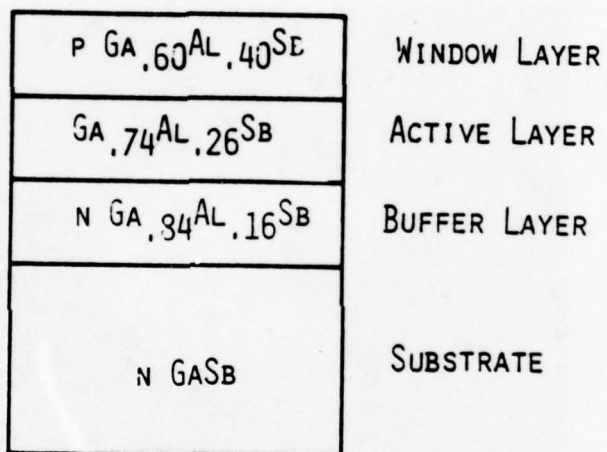


Fig. 22 Structure Of The GaAlSb Avalanche Photodiodes.

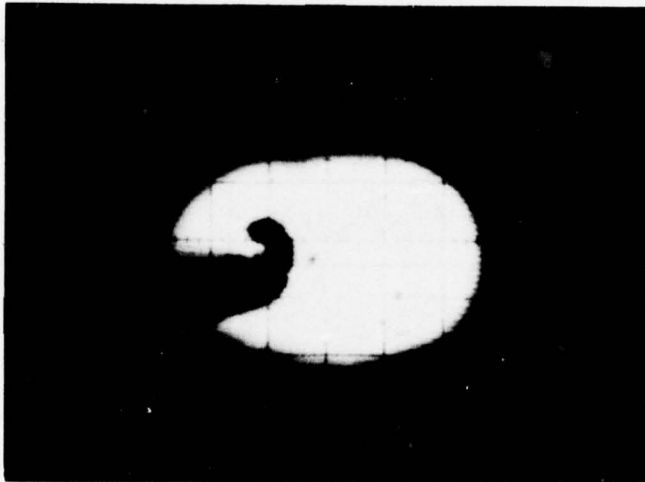


Fig. 23 An Intensity Modulated Scan (The Photocurrent Is Intensity Modulated) Over F10B1S1-G5 At A Gain Of 10, Indicating A Very Uniform Field Inside The Diode.

more closely, we scan the diode and look at the photocurrent at various parts of the diode. Figure 24 shows the results of the traces. The upper trace of the picture is the one with a gain of approximately 18. Most of the bumps are inherited from the low bias curve (the lower trace), implying different light absorption at different parts of the diode. (This might be due to the incident angle difference on various parts of the diode which is not AR coated). In fact, this picture shows an average gain of 17.9. The minimum gain is 13.3 at line b-b' and the highest gain is 20.3 at line a-a'.

Electric field uniformity inside a diode is usually a good indication of the quality of the junction. Nonuniform fields can be caused by bad nucleation, dislocations, nonuniform doping or nonuniform thickness in the material. By expressing the gain factor to the first order of the electric field, one obtains:

$$\frac{1}{M} = \frac{1}{M_0} + E_0 \left( \frac{\Delta E}{E_0} \right) \left( -\frac{\partial(1/M)}{\partial E} \right)_{E = E_0} \quad (1)$$

where M is the gain factor,  $E_0$  the field of interest,  $M_0$  the multiplication at  $E=E_0$ . Therefore, the fluctuation of the electric field will be

$$\frac{\Delta E}{E_0} = \frac{M_0 - M}{M_0 M} \left( \frac{1}{E_0 (\partial(1/M)/\partial E)_{E = E_0}} \right) \quad (2)$$

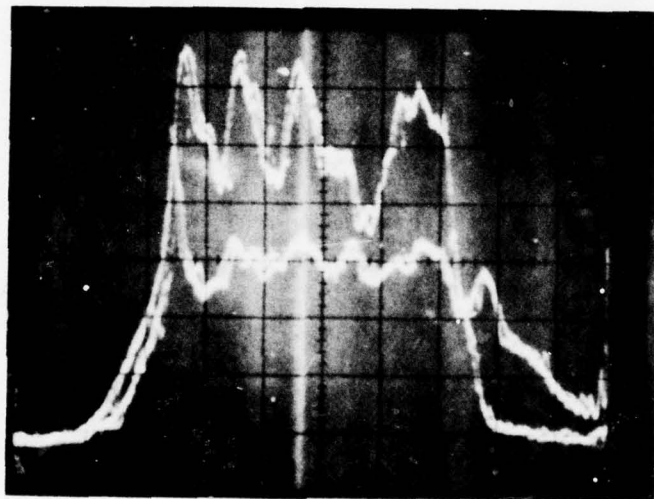


Fig. 24 A Scan Cross-Section Of F10B1S1-G5. Upper Trace Has 10X Attenuations.  $M=17.9$ ; Min.  $M=13.3$ ; Max  $M= 20.3$ .

For the first order of approximation, let us assume equal ionization rates, i.e.  $\alpha = \beta$ . Then, the following is true:

$$1 - \frac{1}{M} = \int_0^w \alpha dx \quad (3)$$

where  $w$  is the depletion width. Thus

$$\frac{\partial(\frac{1}{M})}{\partial E} = \frac{-\epsilon}{qN} \int_0^{E_0} \left(\frac{d\alpha}{dE}\right) dE \quad (4)$$

where at  $x = 0$ ,  $E = 0$  at  $x = w$ ,  $E = E_0$ , and  $N$  is the doping of the active layer. Therefore, one can calculate the fluctuation of the electric field inside the diode by measuring the fluctuation of its gain.

The fluctuation of gain measured from Fig. 24 at 18.1 V bias ( $4.12 \times 10^5$  V/cm) can be used to infer fluctuation of electric field. The fluctuation of the electric fields in F10B151-G5 are found to be +0.12% and -0.34%. This is very uniform.

The dark current of the GaAlSb diode is comparable to that in GaAsSb diodes. Some diodes have a breakdown voltage as high as 70 V which corresponds to a doping of  $n = 4 \times 10^{15} \text{cm}^{-3}$ . This result is encouraging because to achieve such low doping in this material, very accurate control of the compensating dopant is required. The risetime of the GaAlSb diode is comparable to the GaAsSb diodes with the same active area thickness. In both cases, the true risetime cannot be measured because of the risetime limitation of the laser mode locker. But the risetime for a 3 mil diameter diode is

certainly less than 60 p sec. Transit time calculations predict a risetime of the order of 20-40 p sec.

The performance of an avalanche photodiode optical receiver is heavily dependent on the excess shot noise of the APD. The excess shot noise, which essentially is the statistical distribution of the multiplication of the carriers, can be characterized by the carrier secondary ionization rates. The larger the difference between the ionization rates of holes and electrons, the lower will be the excess shot noise (assuming the carriers of the higher ionization rate are photogenerated as primary carriers). Therefore, the ionization coefficients of the electrons and holes in  $\text{Ga}_{0.74}\text{Al}_{0.26}\text{Sb}$  were studied.

The block diagram of the experimental setup for the ionization rate measurement is shown in Fig. 25. In order to make accurate measurement, pure electron and pure hole injection into the same junction are essential. The structure of the diode suitable for pure injection is shown in Fig. 26. A  $0.63\mu\text{m}$  He-Ne laser is used to inject electrons into the junction. The laser light is strongly absorbed in the first layer and the electron-hole pairs are excited there. The created electrons will then diffuse into the junction and start the multiplication process. A  $1.15\mu\text{m}$  He-Ne laser is used to inject holes into the junction. The first two layers are transparent to  $1.15\mu\text{m}$  radiation which eventually will be absorbed in the third layer. The created holes will diffuse back to the junction and start the multiplication. Subsequently, curves of  $M_n$ , electron multiplication and  $M_p$ , hole multiplication, vs bias voltage are taken.

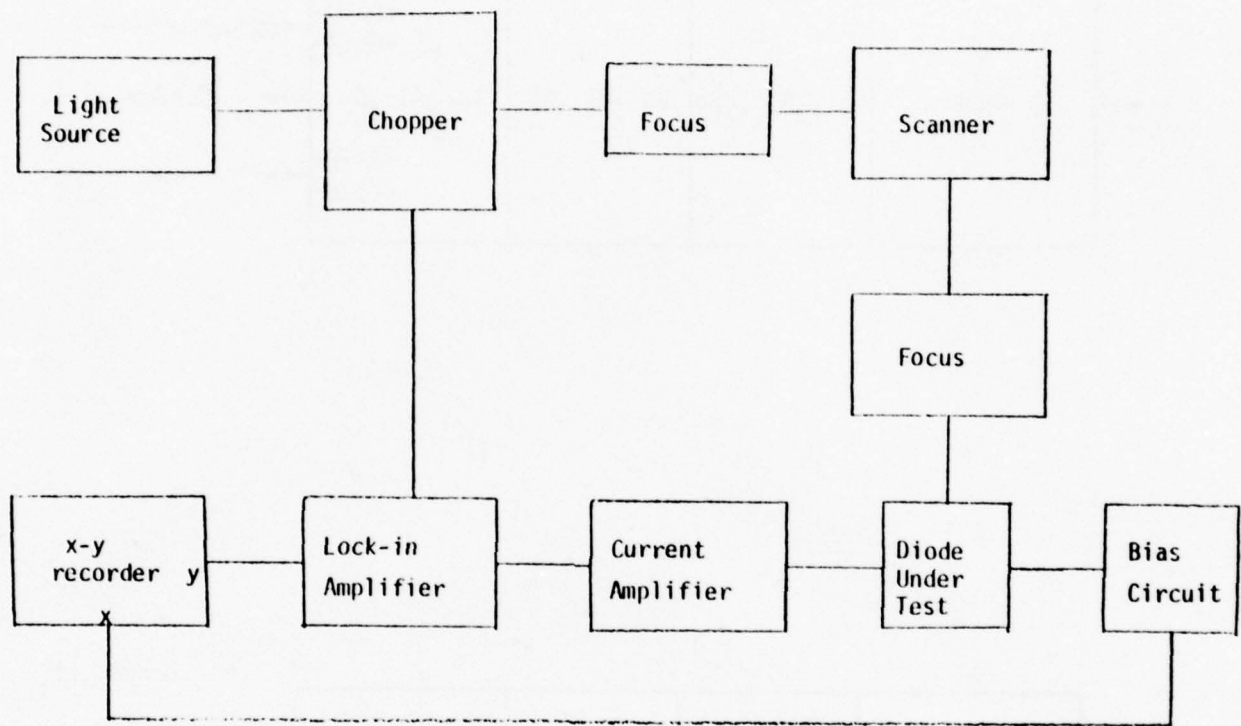


Fig. 25 Block Diagram Of Ionization Coefficients Measurement.

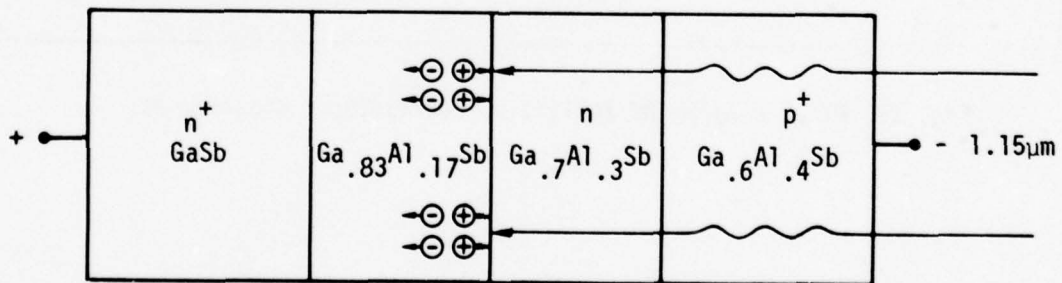
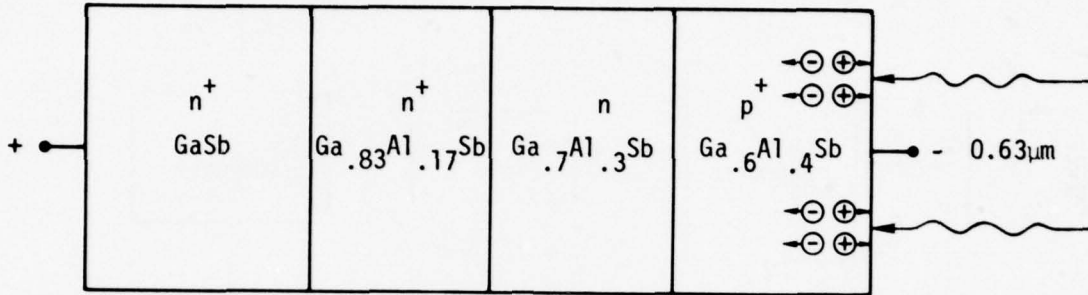


Fig. 26 Structure Of GaAlSb Diodes Suitable For Pure Carrier Injection.

The relations between  $\alpha$ , the electron ionization coefficient,  $\beta$ , the hole ionization coefficient and  $M_n$ ,  $M_p$  are as follows:

$$1 - \frac{1}{M_n} = \int_0^w \alpha \exp\left[-\int_0^x (\alpha - \beta) dx'\right] dx \quad (5)$$

$$1 - \frac{1}{M_n} = \int_0^w \beta \exp\left[\int_x^w (\alpha - \beta) dx'\right] dx \quad (6)$$

$$\ln \frac{M_n}{M_p} = \int_0^w (\alpha - \beta) dx \quad (7)$$

where  $w$  is the depletion width.

For a one-sided abrupt junction with constant doping on the active layer and under the non-punch through condition, the above equations can be solved with suitable boundary conditions:

$$\alpha(E_m) = E_m \left\{ \frac{d(\ln M_n)}{dV} - \frac{M_n - 1}{M_n} \cdot \frac{d(\ln M_p)}{dV} \right\} \quad (8)$$

$$\beta(E_m) = \frac{E_m}{M_n} \frac{d(\ln M_p)}{dV} \quad (9)$$

where  $E_m$  is the maximum electric field and  $V$  the bias voltage.

The space charge widening effect can be corrected by best fitting the low bias photocurrent to the following function:

$$J_p = \frac{A}{\cosh\left(\frac{\ell-w}{L}\right)} \quad (10)$$

where  $J_p$  is the photocurrent,  $A$  a constant,  $L$  the diffusion length of holes in n-type material,  $\ell$  the length of the active layer, and  $w$  the depletion width.

The ionization rates of  $\text{Ga}_{0.74}\text{Al}_{0.26}\text{Sb}$  were measured in five different samples, F10B1S1-G5, F10B1S1-G6, F10B1S1-G7, F10B1S1-GC1 and F10B1S1-GC2. The doping of the materials was measured by capacitance-voltage method and found to vary from  $7.0 \times 10^{15} \text{cm}^{-3}$  to  $4 \times 10^{16} \text{cm}^{-3}$  covering a wide electric field range for the data. The diodes used in this measurement have all been checked for junction uniformity. The deduced ionization rates were plotted in Fig. 27. A consistent result  $\beta/\alpha$  approximately 2 is found.

The numerical constants of  $\alpha$  and  $\beta$  are

$$\alpha = 1.04 \times 10^5 \exp\left[-(4.10 \times 10^5/E)^2\right]$$

$$\beta = 1.91 \times 10^5 \exp\left[-(4.12 \times 10^5/E)^2\right]$$

Where  $\alpha, \beta$  are in units of  $\text{cm}^{-1}$  and  $E$  is Volts/cm.

The breakdown voltages of a one-sided abrupt junction uniformly doped n-type diode can be calculated by integrating the above ionization rates. The result is shown in Fig. 28. The I-V characteristics measured on a curve tracer agree closely with the calculated breakdown voltage. This self

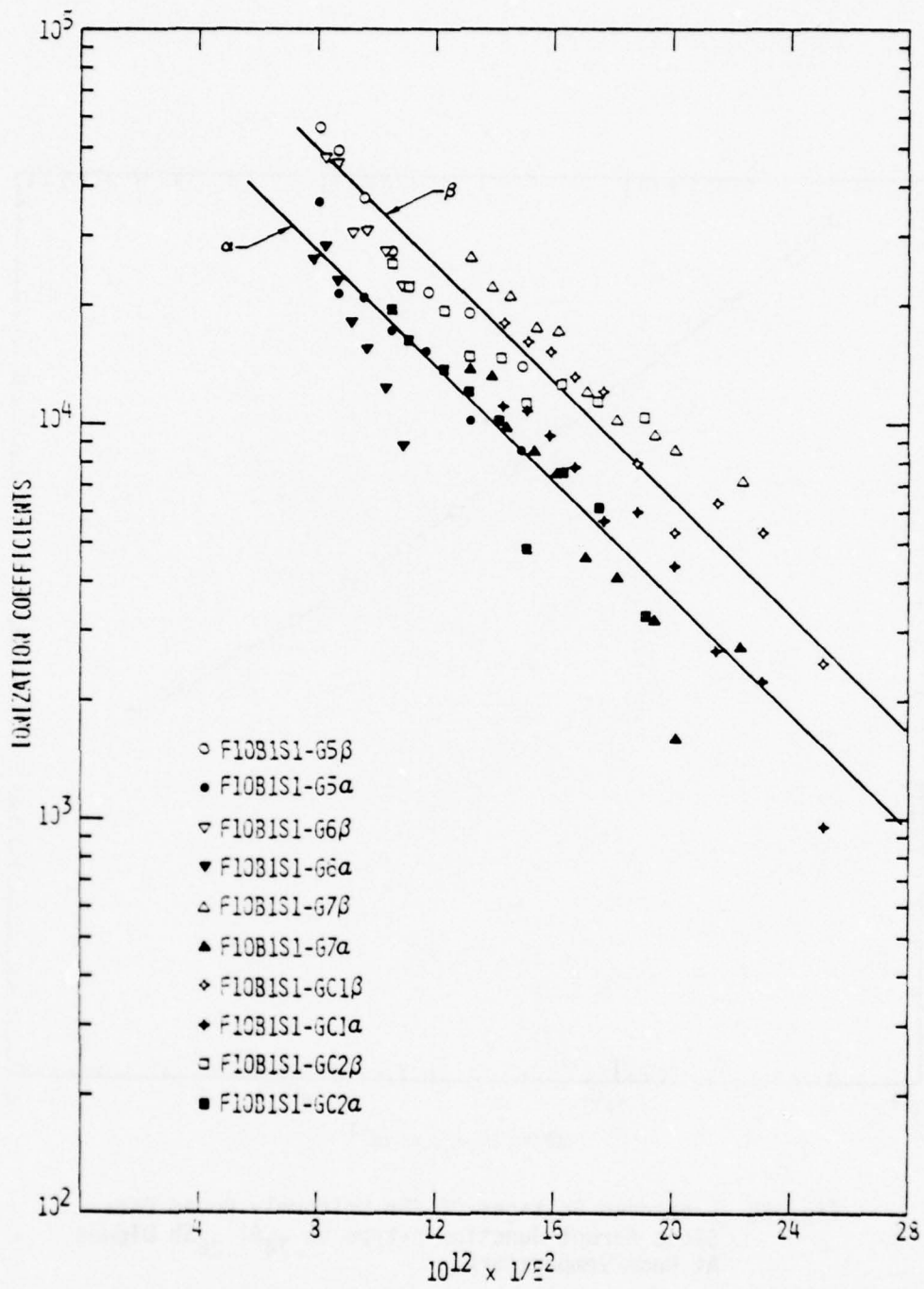


Fig. 27 Ionization Coefficients For  $\text{Ga}_{.74}\text{Al}_{.26}\text{Sb}$ .

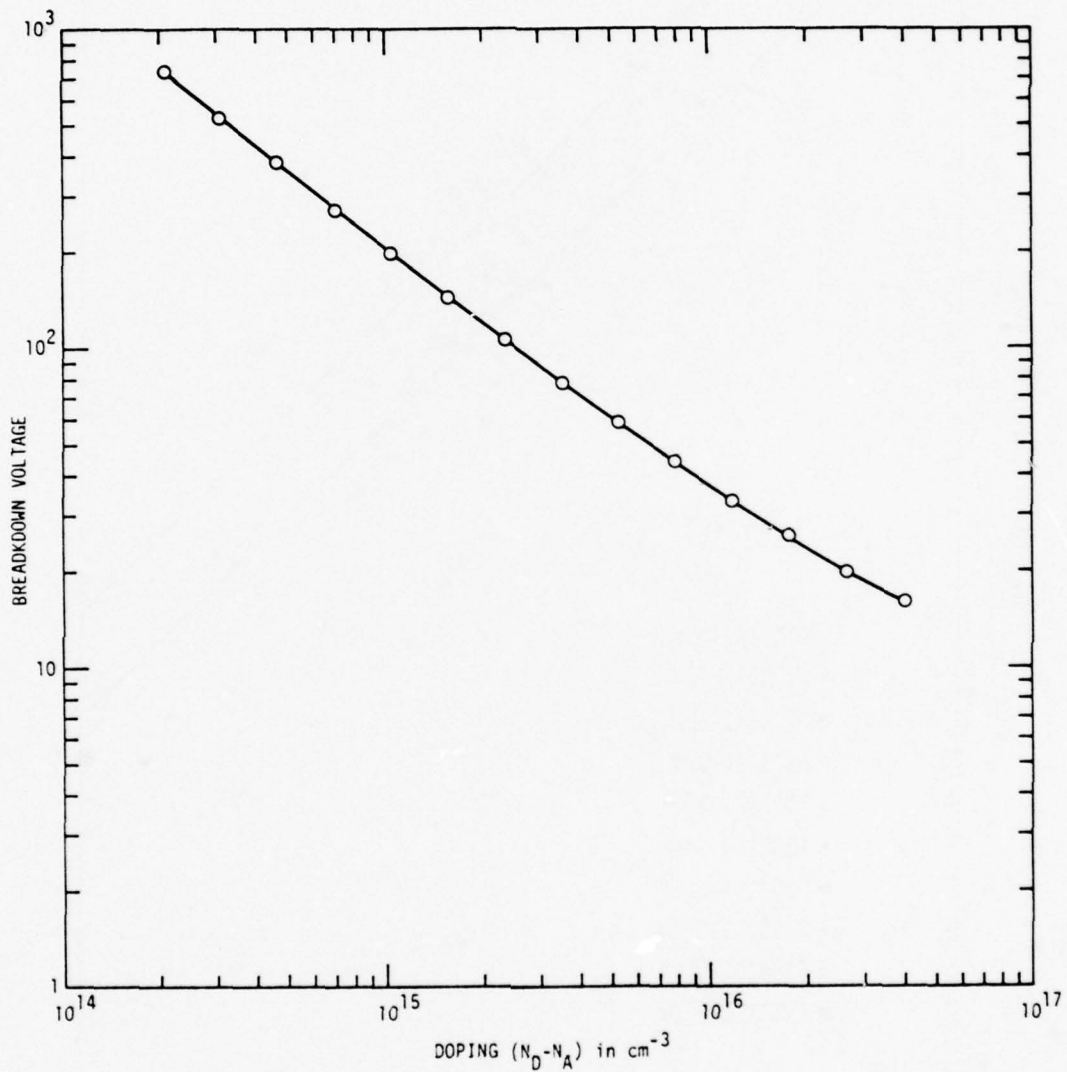


Fig. 28 Breakdown Voltages Of The Uniformly Doped One-Sided Abrupt Junction n-type  $\text{Ga}_{.74}\text{Al}_{.26}$  Sb Diodes At Room Temperature.

consistency substantiates the good quality of these diodes and the validity of the ionization rate measurement.

The excess noise factor of a  $\text{Ga}_{0.74}\text{Al}_{0.26}\text{Sb}$  avalanche photodiode is estimated to be equal to 0.75 based on the calculations of McIntyre<sup>7</sup> and this ionization coefficients measurement. The excess noise of GaAlSb diode is comparable to GaAsSb  $1.06\mu\text{m}$  APD, and is better than GaAs (where  $X_n \approx 1$ ). No large anisotropy of ionization rates has been found in any III-V semiconductor. Unlike the case of silicon, the  $\alpha/\beta$  or  $\beta/\alpha$  ratio in all III-V is limited to 5 or less. The III-V avalanche photodiode is still superior to the silicon avalanche photodiode because of their high quantum efficiency due to being direct bandgap materials.

The present limitation on the GaAlSb avalanche photodiode performance is surface breakdown. Unlike the GaAsSb diode, in which the gain is limited by hot spots inside the junction, the GaAlSb diode has a sharp increase in surface leakage current as the bias is increased. The use of anodic oxidation passivation will be attempted to reduce the surface leakage.

### 3.2.2 Light Emitting Diodes

In order to complete an optical communication system, a high radiance light emitting diode is required. The InGaAsP/InP and GaAlAsSb/GaAsSb systems are the candidates at  $1.06\mu\text{m}$ .

The lifetime of the light emitting diode is a major research area to improve the reliability of the transmitting system. The degradation of the performance of the LED is mostly caused by the growing and migrating of the dark spots caused by crystal defects. The dark spots are high current

filimentary paths which do not emit light, lower the efficiency, elevate the operation temperature of the LED and thus shorten its lifetime. At the high current density levels required for LED operation, even a small amount of series resistance caused by imperfect ohmic contacts reduces LED performance by raising the junction temperature by  $I^2R$  heating. Six layer structure LEDs in the GaAlAsSb/GaAsSb system were built. In order to achieve long life LEDs, the interfaces and lattice match between the GaAlAsSb confinement and GaAsSb active layers must be nearly perfect. To decrease the dislocation density in the active region of the LED, three intermediate composition layers of  $\text{GaAs}_{1-x}\text{Sb}_x$  with  $x = 0.02, 0.05$  and  $0.08$  are grown before the confinement and active layers. This dramatically improves the lattice match.

Double heterostructure LEDs of this system is shown in Fig. 29. The thickness of each of the layers is as follows: 1)  $\text{GaAs}_{.98}\text{Sb}_{.02}$ ,  $t = 8.2\mu\text{m}$ , 2)  $\text{GaAs}_{.95}\text{Sb}_{.05}$ ,  $t = 4.3\mu\text{m}$ ; 3)  $\text{GaAs}_{.92}\text{Sb}_{.08}$ ,  $t = 4.3\mu\text{m}$ ; 4)  $\text{Ga}_{.75}\text{Al}_{.25}\text{As}_{.91}\text{Sb}_{.09}$ ,  $t = 3.9\mu\text{m}$ ; 5)  $\text{GaAs}_{.91}\text{Sb}_{.09}$ ,  $t = 1\mu\text{m}$ ; 6)  $\text{Ga}_{.75}\text{Al}_{.25}\text{As}_{.91}\text{Sb}_{.09}$ ,  $t = 2.6\mu\text{m}$ . The lattice constant and composition of the top confinement and active layers was confirmed to be  $\text{GaAs}_{.909}\text{Sb}_{.091}$  by Gandolfi measurements. The layer quality is excellent with no indication of large dislocation concentration at the interfaces.

Front surface emitting LEDs were fabricated from the above multi-epitaxy structures. The diodes were etched mesa structures with a circular ring ohmic contact around the outer edge with light emitted inside this ring. The electroluminescence spectrum for one of these diodes is shown in Fig. 30. The room temperature peak emission is at  $1.035\mu\text{m}$  with a  $420\text{\AA}$  FWHM

Confining Layer  $\text{Ga}_{.7}\text{Al}_{.3}\text{As}_{.91}\text{Sb}_{.09}$ ;  $P = 2 \times 10^{18}$

---

Active Layer  $\text{GaAs}_{.91}\text{Sb}_{.09}$ ;  $P = 2 \times 10^{17}$

---

Confining Layer  $\text{Ga}_{.7}\text{Al}_{.3}\text{As}_{.91}\text{Sb}_{.09}$   $n = 1 \times 10^{18}$

---

3rd Matching Layer  $\text{GaAs}_{.92}\text{Sb}_{.08}$   $n = 1 \times 10^{18}$

---

2nd Matching Layer  $\text{GaAs}_{.95}\text{Sb}_{.05}$   $n = 1 \times 10^{18}$

---

1st Matching Layer  $\text{GaAs}_{.98}\text{Sb}_{.02}$   $n = 1 \times 10^{18}$

---

$n^+$  GaAs Substrate

---

Fig. 29 Schematic Of Six Layer Double Heterostructure GaAlAsSb/GaAsSb LED.

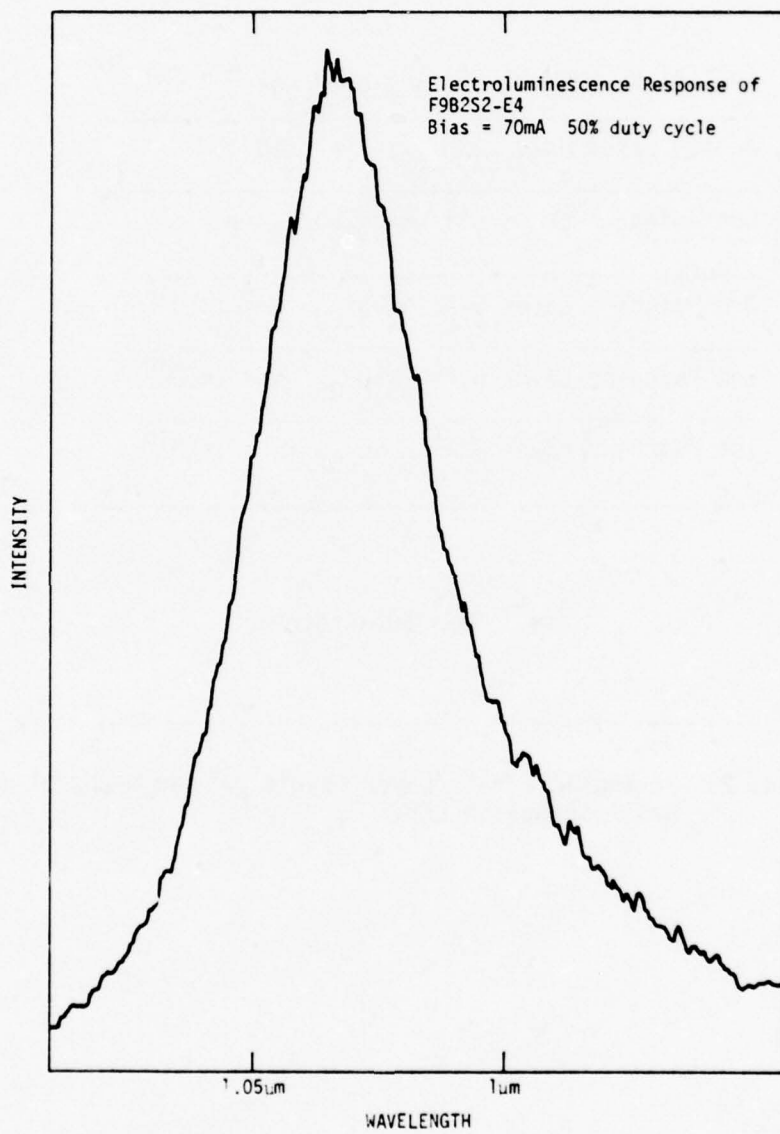


Fig. 30 Electroluminescence Measurement Of The Ga<sub>1</sub>AsSb/GaAsSb LED.

bandwidth. This is the first successful double heterostructure LED emitting at  $> 1\mu\text{m}$  which we have fabricated and tested.

One of the potential applications of fiber systems is analog data transmission. Analog systems require a high degree of linearity in both the source and detector to transmit and reproduce the signal accurately. The linearity of these diodes was measured with the luminescence spectrometer. The spectrometer was set to the peak wavelength at  $1.035\mu\text{m}$  and the photomultiplier current measured as a function of LED bias current. The relative light output vs drive current is shown in Fig. 31. At low bias the diode is not linear, however, for bias currents between 10mA and 200mA, the diode linearity is excellent and would easily permit analog signal transmission with good fidelity.

In the InGaAsP/InP system, preliminary crystal growth shows exceedingly encouraging results. Exact lattice match, double heterostructure layers with excellent surface morphology were obtained. The schematic of layers are shown in Fig. 15. It consists of: 1)  $n^+$  InP substrate; 2)  $n = 2 \times 10^{18}$  InP confining layer; 3)  $n = 2 \times 10^{17}$  In<sub>0.89</sub>Ga<sub>0.11</sub>As<sub>0.25</sub>P<sub>0.75</sub> active layer with a thickness of  $1\mu\text{m}$ ; 4)  $p = 2 \times 10^{18}$  InP confining layer.

Both front surface emitting and substrate emitting LED have been fabricated from these layers. The substrate emitting structure has an advantage over the front surface emitting one because the active layer of the former is closer to the heat sink and will operate closer to the ambient. The light spectrum from these LEDs are shown in Fig. 32. At room temperature, the emission peaks are at  $1.05\mu\text{m}$ .

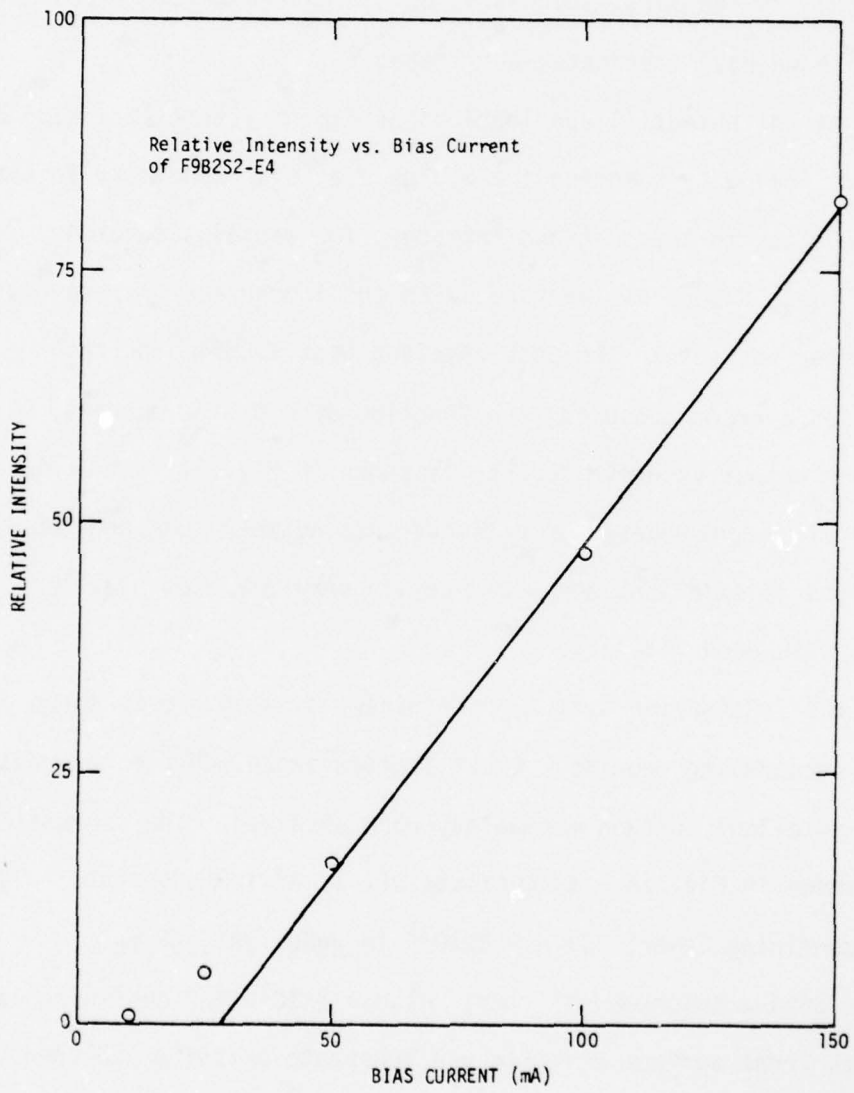


Fig. 31 Intensity vs. Bias Current Of GaAlAsSb/GaAsSb LED.

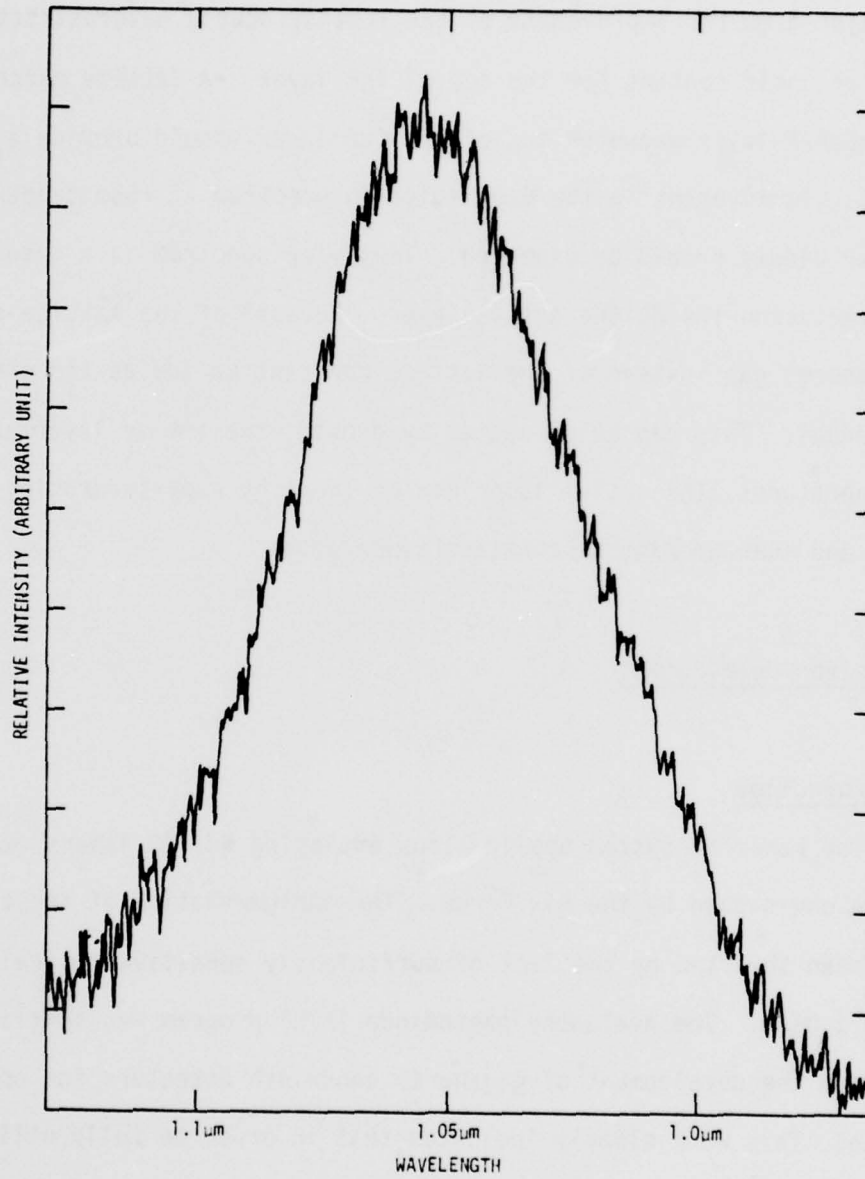


Fig. 32 Electroluminescence Measurement Of The InGaAsP/InP LED.

A major area for improvement of the InGaAsP double heterostructure LED is a better ohmic contact for the top  $p^+$  InP layer. A lattice matching quaternary InGaAsP layer grown on top of the InP layer should provide a better ohmic contact. Improvement in the wide emission spectrum at room temperature of the InGaAsP diodes should be expected. This wide spectrum is a result of composition variation inside the active layer. Because of the lattice pulling effect, the energy gap instead of the lattice constant varies as the growth temperature drops. This can be corrected by growing the active layer at constant temperature. The active layer can be grown by supersaturating the melt by  $10^{\circ}\text{C}$  and then growing at constant temperature.

### 3.3 Receiver Development

#### 3.3.1 Introduction

A wide range of system applications employing Nd:YAG lasers emitting at  $1.06\mu\text{m}$  are envisioned by the Air Force. The implementation of these systems has been thwarted by the lack of sufficiently sensitive optical detectors at  $1.06\mu\text{m}$ . The avalanche photodiode (APD) program was initially directed toward the development of gigahertz bandwidth detectors for optical communication. This work clearly indicated that in order to fully utilize the tremendous speed potential available in III-V APDs, it is essential to operate them as the sensing elements in integrated (hybrid) receivers. The following circuit elements and circuit design must be carefully thought out for each application to take full advantage of superior APD performance, thus assuring maximum possible system performance.

The two distinct system applications considered here are a laser illuminated line scan system and a gigabit communication receiver. These two system requirements will be addressed by three distinct receiver designs, a DC-5 MHz baseband receiver, a 5 MHz bandwidth receiver tuned at 100 MHz, and a gigabit data rate digital receiver. The first two receivers are alternate approaches to the problem of an ultra-sensitive airborne laser line scan system.

Previous work on Air Force Contracts No. F33616-75-C-1165 and F33615-76-C-1011 has been funded to study the DC-5 MHz receiver, while Air Force Contract No. F33616-74-C-1030 as well as NASA Contract No. NAS5-23134 were aimed at the high data rate receiver technology. The 100 MHz tuned receiver work was initiated under the present contract. The receivers in question all share the same basic detector requirements: high speed, high quantum efficiency, low dark current, low excess multiplication noise factor and moderate but uniform avalanche multiplication factors. With the APD device results described in the previous section the device requirements for superior receiver performance are now available. The following sections describe the expected performance of the three receivers based on actual photodiode measurements and previous receiver contract work.

3.3.2 DC-5 MHz 1.06 $\mu$ m Receiver For Laser-Illuminated Airborne Night Imaging "Laser Line Scan" Systems

The requirements for "Laser Line Scan" System are:

S/N = 5 in 5 MHz bandwidth (desired)

S/N = 3 in 3.5 MHz bandwidth (minimum)

$P_r \approx 10^{-9} \text{w}$

$m = .4$  (modulation index)

The signal to noise ratio can be written as

$$\frac{S}{N} = \left( \frac{m\sqrt{2} M \frac{q\eta P_L}{h\nu}}{2 + X_n \left( \frac{q\eta P_L}{h\nu} + I_B \right) + i_{nj}^2 + i_{ne}^2} \right)^{1/2}$$

where

$P_L$  is the optical power

$I_{nj}$  is the Johnson noise current

$I_{ne}$  is the amplifier noise current

$M$  is the avalanche gain

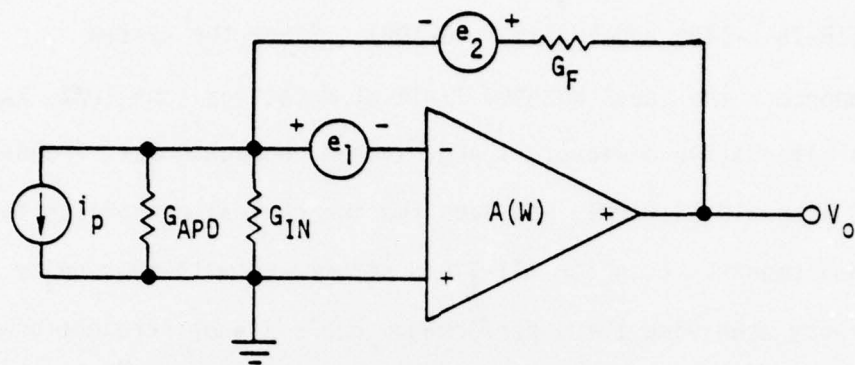
$h\nu$  is the photon energy

$\Delta f$  is the electrical bandwidth

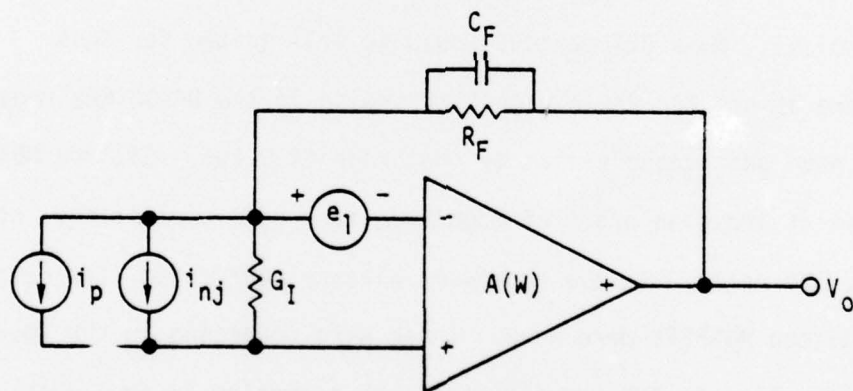
$I_B$  is the bulk leakage current

$X_n$  is the excess avalanche noise factor

The circuit configuration is the transimpedance feedback design shown in Fig. 33 and described in detail in the final reports for Air Force



(a)



(b)

Fig. 33 Model Used For Analysis Of Signal And Noise Response.  $e_1$  Is The Equivalent Input Noise Voltage Generator Of The Preamp,  $e_2$  Is The Johnson Noise Voltage Generator Of The Conductance  $G_F$ . In (b),  $G_I$  Replaces The Input Conductance Of The Preamp And The Conductance Of The APD And  $i_{nj}$  Replaces  $e_2$ .

Contracts F33615-75-C-1165 and F33615-76-C-1001. Since the system requirements approach the ideal quantum limit of detection ( $\eta = 100\%$ ,  $X_n = 0$ ) none of the alternative devices, Si APD,  $1.06\mu\text{m}$  photocathodes, frequency doubled Nd:YAG with a  $0.53\mu\text{m}$  PMT, has even the theoretical capability to meet the system requirements. Even for III-V APD structures with near unity quantum efficiency achieving these performance goals is not straightforward. Equation (11) clearly shows the importance of  $X_n$  when performance is signal shot noise limited. The final report for F33615-75-C-1165 pointed out the significance of preamplifier input capacitance in determining noise levels when M is small. The preamplifier input capacitance is limited by silicon and GaAs FET technology. GaAs FET devices would be well suited for this application were it not for their high "1/f" noise in the DC-10 MHz region. These devices have gate capacitances of the order of 0.2pF. Silicon MOSFET devices exhibit at least an order of magnitude more gate capacitance; however, they have low, 1/f noise. In the receivers already fabricated, low noise, low capacitance silicon MOSFETs were used. These were connected in the source follower configuration to take advantage of the reduction in equivalent input capacitance these circuit configurations provide.

Using GaAs APDs discussed in the previous section, we calculate the signal to noise performance of the laser line scan receiver using measured detector and circuit parameters.

The parameters used are:

$$X_n = .75$$

$$I_B = .5\text{nA (measured in AFAL-TR-76-113)}$$

$$\eta = 80\% \text{ (reported in previous section)}$$

$$e_n = 5\text{nv/Hz (measured in AFAL-TR-76-113)}$$

$$I_{ne} = 2 \times 10^{-19} \text{A}^2 \text{ (measured in AFAL-TR-76-113)}$$

$$P_r = 1\text{nW (assumed condition)}$$

Figure 34 shows the results of the calculations. Shown on the figure are points representing previously reported results with avalanche gain, a Si APD with  $\eta = 15\%$  and  $X_n = .4$  driving the same preamplifier as the III-V APD, an idealized  $1.06\mu\text{m}$  PMT with  $\eta = 1\%$  and the frequency doubled  $0.53\mu\text{m}$  PMT system which has  $\eta = 20\%$  for the PMT and a 67% power conversion from  $1.06\mu\text{m}$  to  $0.53\mu\text{m}$ . The net efficiency of the doubled system is 7%.

The results reaffirm previous analyses that the required receiver performance can only be achieved with III-V APDs. The III-V APDs are at least 3 dB better than Si APDs. The added complexity of operating and aligning  $1.06\mu\text{m}$  doublers and  $0.53\mu\text{m}$  PMT makes that system choice undesirable. For the 3.5 MHz bandwidth case, desired receiver performance ( $S/N = 3$ ) can be achieved with 1.1nW of optical power a mere 10% above specifications. It should be pointed out that these results are based on conservative estimates of  $X_n$  and and represent the minimum performance that will be achieved.

### 3.3.3 5 MHz Bandwidth, 100 MHz Tuned Receiver for Airborne Laser Line Scan System

In this approach to the Laser Line Scan System, the scene illuminating laser is mode-locked with a 100 MHz repetition frequency rather than the CW operation utilized in the baseband receiver described in the last section. The disadvantage of the baseband system is that its performance is degraded by background such as moonlight or sunlight. This problem is substantially reduced with a mode locked laser approach. Here, the only

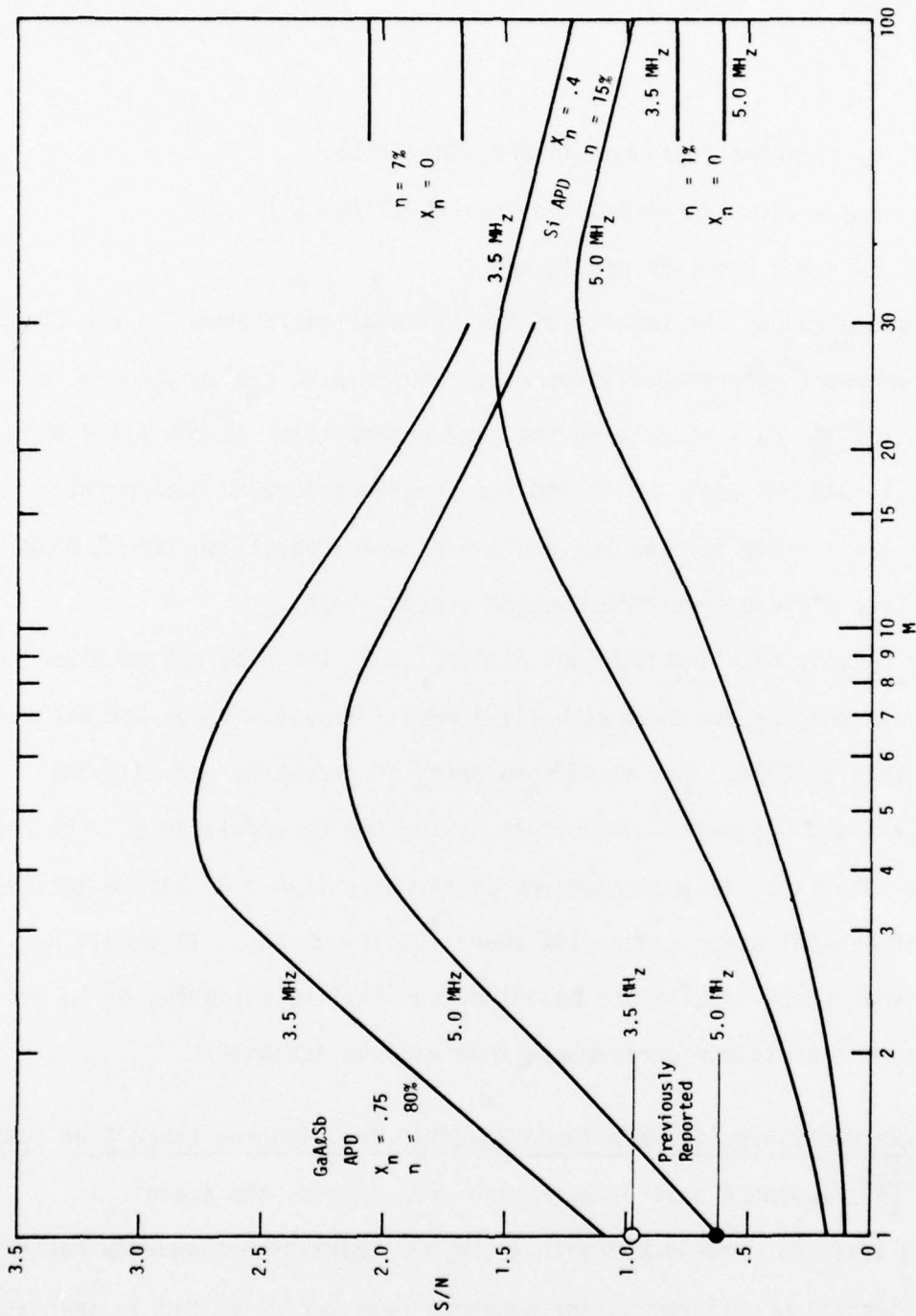


Fig. 34 Signal-To-Noise Ratio Versus Gain For The Base Band Laser Line Scan Receiver.

background noise will be the 100 MHz contribution due to scanning over fluctuations in scene brightness with a mode locked laser and a suitable receiver, range height variations can also be determined. From the electronic circuit standpoint, high speed, low noise GaAs FETs can now be used because the "1/f" noise is insignificant at 100 MHz.

The design approach utilized for the baseband receiver is not appropriate, since the noise contribution due to the preamp ( $i_{ne} \propto e_n C_i \omega$ ) would be quite large at  $\omega/2\pi = 100$  MHz. The optimum approach here is a high 'Q' resonant circuit composed of the capacitance of the APD and an inductor. In this circuit, the APD is operated as the capacitor in the resonant circuit. This concept has the decided advantage that the signal to noise ratio becomes approximately proportional to the 'Q' of the circuit.

A prototype of such a circuit (tuned to 300 MHz) was built, evaluated, and delivered to the Air Force as part of Contract No. F33601-74-C-0498. This receiver was built to demonstrate the concept and was not optimized. Even so, in a comparison with a selected S-1 photomultiplier, it performed about 17 dB better.

The performance of an RLC tuned circuit will result in better signal to noise performance simply because better (lower noise) semiconductor devices can be used. In the previous section describing the DC-5 MHz receiver, GaAs FET devices could not be used because of severe "1/f" noise restrictions. At 100 MHz the "1/f" noise is negligible and therefore the superior  $e_n$  and  $C_{in}$  characteristics of GaAs can be utilized. With  $e_n = 1_{nV}/\sqrt{\text{Hz}}$  and  $C_{in} \leq 0.3\text{pF}$  noise performance at unity avalanche gain ( $M=1$ ) is dominated by Johnson noise.

Figure 35 shows the results for (S/N) vs M for the same APD and signal parameters used for the DC-5 MHz line scan system. The performance of the 100 MHz tuned receiver is superior to the baseband system by nearly 20%. The minimum signal to noise and bandwidth requirements can be met with existing APD technology. Further improvement is expected in APDs as the 1.06 $\mu$ m materials being studied are improved.

#### 3.3.4 Gigabit Data-Rate 1.06 $\mu$ m Laser Communication Receiver

This system requires an optical receiver for the detection of modelocked laser pulses with 1 GHz repetition frequency(1ns separation). The best performance demonstrated anywhere to date for such a system has been by the GaAsSb avalanche photodiode-GaAs FET preamp receiver built at the Science Center under Air Force Contract No. F33615-74-C-1030.

The best of these receivers required, for a bit error rate of  $10^{-6}$ , a minimum of  $N_p = 3400/M$  photons per bit, where M is the avalanche gain (valid for low M). The improvement in this receiver comes from the improved avalanche gain and gain uniformity.

Figure 36 shows the performance for the 1 GB/sec system for an  $X_n = 0.25$  APD and reported Science Center GaAs FET preamp performance. Using an  $X_n = 0.75$  GaAsSb APD performance for  $M < 20$  is as shown in Fig. 36. the optimum performance of  $N_p < 200$  photon occurs at an avalanche gain of  $M=18$ . For larger gain, performance degrades because of the excess avalanche gain noise.

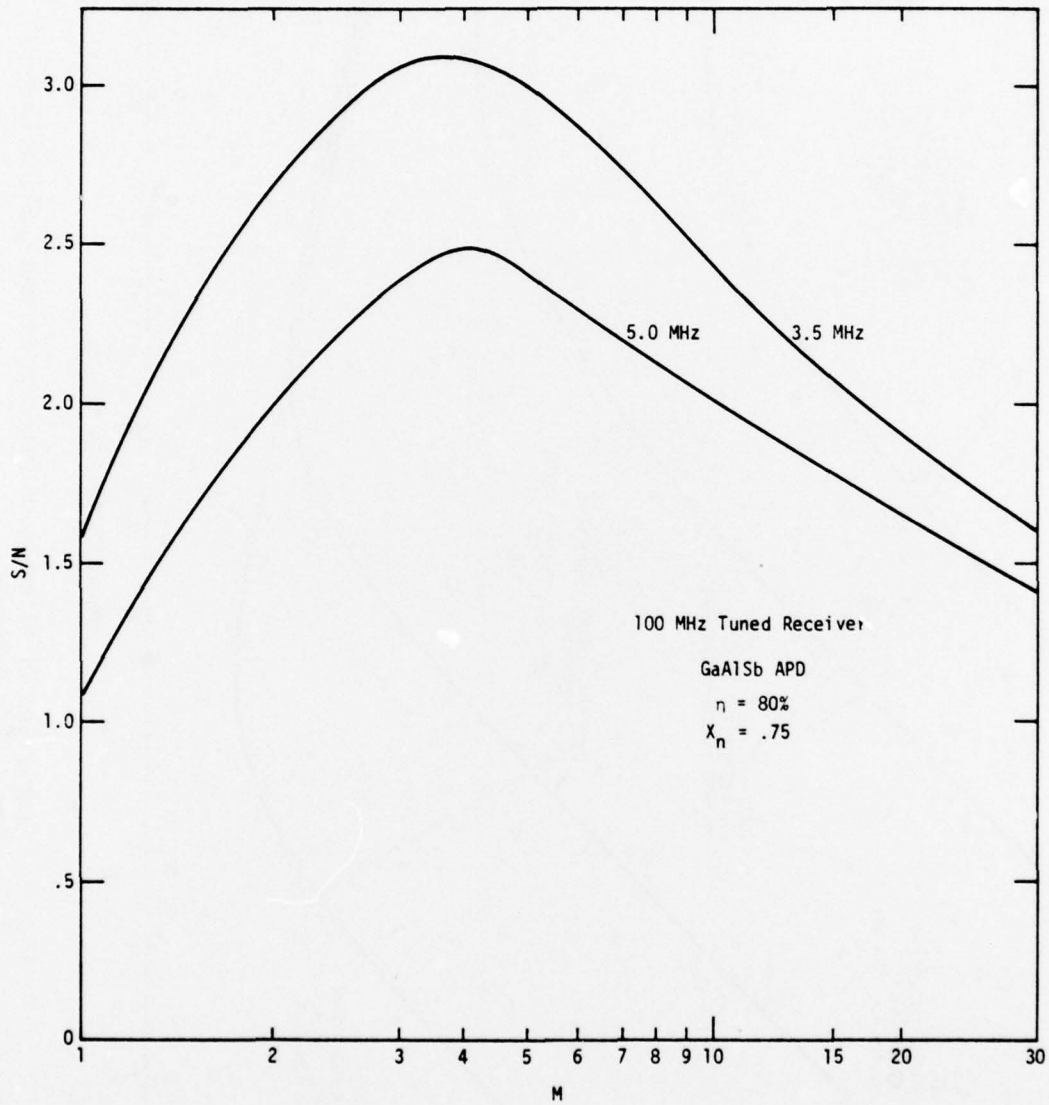


Fig. 35 Signal-To-Noise Ratio Versus Gain For The 100 MHz Tuned Laser Line Scan Receiver.

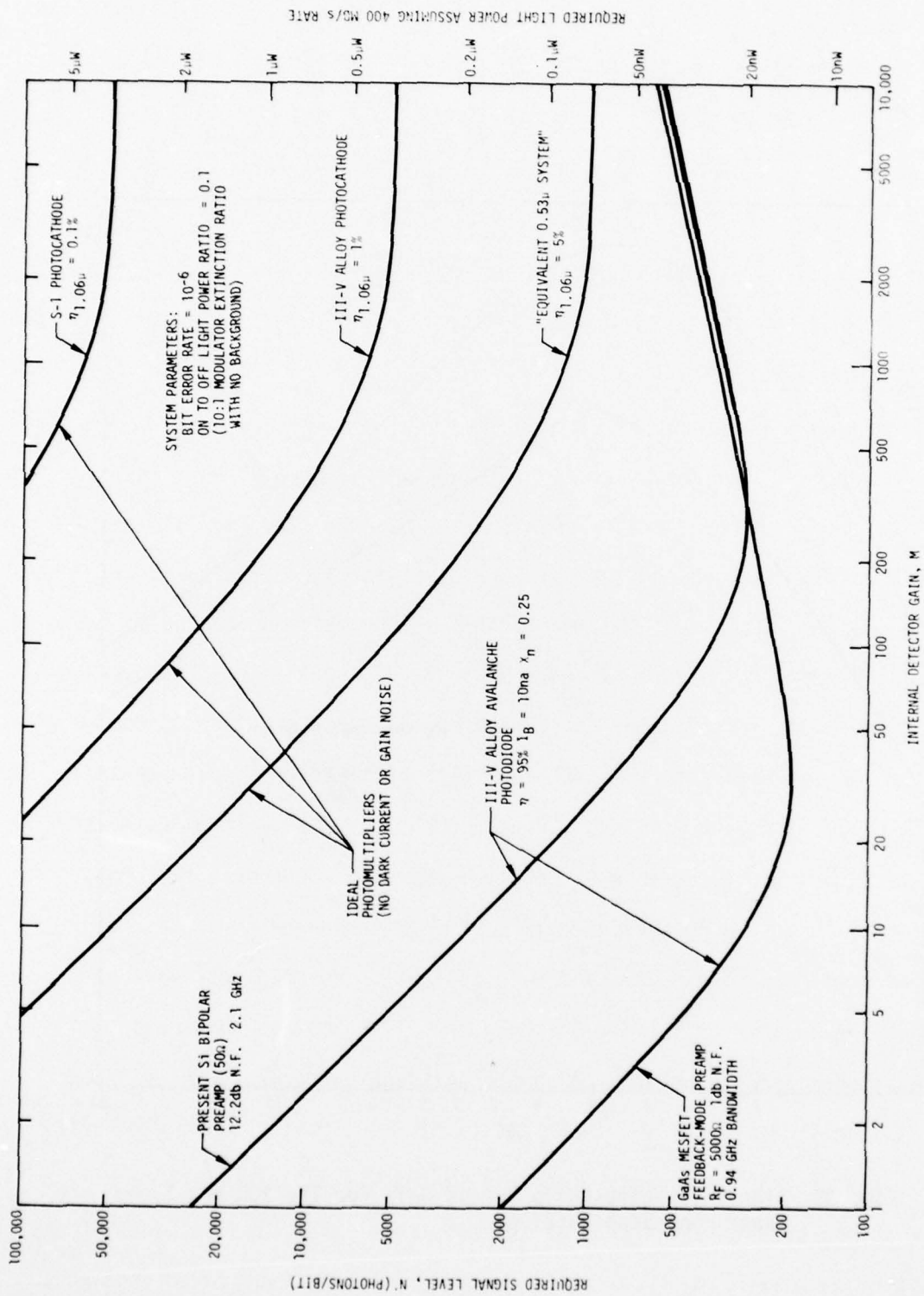


Fig. 36 Comparison Of Alternative Detector-Preamp Combinations  
 For 1 GB/s Receiver.

SECTION IV  
SUMMARY AND CONTINUING RESEARCH

4.1 Summary of Results

The most significant results to date have been concentrated in the material and device development area. In the material area three alloys systems have been explored, GaAsSb, GaAlSb and InGaAsP. The high dislocation density of GaAsSb has been reduced by a series of lattice matching layers. An intensive study of dopants in this material has been made and doping control to the low  $10^{15}\text{cm}^{-3}$  has been achieved. A doping drop method has been developed to reduce interface defects and compositional variation in the grown layer. In the GaAlSb system the better lattice match between epilayer and substrate results in a very smooth surface morphology. Avalanche photodiodes fabricated from this system show extremely uniform photoresponse over the entire optically active area even at microwave avalanche gains as high as 20. A detailed study of the electron and hole ionization coefficients have been made and indicate a factor of two differences. This implies an excess multiplication noise factor of 0.75 which, although larger than the silicon (0.4), is significantly smaller than GaAs (1.0). The most promising material system is the InGaAsP quaternary. In this system the epilayer lattice constant is "forced" to match that of the substrate. The best surfaces of any III-V system have been achieved in the quaternary. LEDs fabricated from grown layers show excellent performance and lifetime tests are currently being initiated.

Avalanche photodetector improvement has been concentrated in the area of improved photoresponse uniformity at moderate avalanche gains. InGaAlSb system high speed ( $t_r < 80\text{ps}$ ), high quantum efficiency ( $\eta > 80\%$ ), detectors with uniform microwave avalanche gains of 16-20 have been achieved. These diodes have the highest speed-quantum efficiency performance reported for any APDs at  $1.06\mu\text{m}$ .

#### 4.2 Material Development

The major materials development effort for the remainder of the contract will be in the InGaAsP system. This material, because it can be perfectly latticed matched, should provide APDs of superior gain uniformity. The fact that it is grown on InP, a wide bandgap material will permit the APDs to be substrate or backside illuminated. The perfect lattice match should also be essential to making superradiant LEDs with long lifetimes. The problems that will be addressed are: doping control, low carrier concentration growth, thickness control, anti-reflection coatings, low resistance contacts and surface passivation procedures. Work will continue on doping level control, passivation and anti-reflection coatings for the GaAlSb system.

#### 4.3 Device Development

Improvements in bulk leakage and gain uniformity will be the major effort for GaAlSb APDs. Since system analysis indicates that a gain of 20 ( $M=20$ ) is sufficient for the three receivers being considered, no great effort will be spend to improve the gain in GaAlSb systems beyond this point.

InGaAsP APDs will be fabricated, their ionization constants, quantum efficiency and leakage currents measured. If superior performance can be expected from InGaAsP APDs for the systems studied, then a concerted effort will be made to optimize the quaternary APDs in order to incorporate them into the receivers.

LED and superradiant LEDs will be fabricated from GaAsSb and InGaAsP layers. Techniques will be developed for growing very thin ( $< 0.5\mu\text{m}$ ) planar active layers with carefully latticed matched confining layers. a reliable, low thermal resistance packaging technique will be developed. The device parameters of chief interest include: external efficiency, risetime, and reliability. Total efficiencies of 2% for LEDs and 20% for superradiant LEDs should be achievable. the major effort on superradiant LEDs will be directed toward fabrication problems. The problems of coupling the optical radiation into a fiber will be examined and suitable structures for efficient coupling developed.

#### 4.4 Receivers

The major receiver work to be carried out is the fabrication, testing, refinement and delivery of the three receivers previously described. This task should occupy the majority of the remaining effort on this contract.

Further analysis of the 100 MHz tuned receiver will be carried out to further improve system performance.

Reference for Air Force Report, Chap. 5.

1. Nahory, R.E., Pollack, M.A., DeWinter, J.C., and Williams, K.M., "Growth and Properties of Liquid Phase Epitaxial  $\text{GaAs}_{1-x}\text{Sb}_x$ ," J. Appl. Phys. 48, 1607, (1977).
2. Waho, T., Ojawa, S., and Maruyama, S., " $\text{GaAs}_{1-x}\text{Sb}_x$  ( $0.3 < x < 0.9$ ) Grown by Molecular Beam Epitaxh," Jap. J. of Appl. Phys. 16, 1875, (1977).
3. Antypus, G.A. and Moon, R.L., "Growth and Characterization of  $\text{GaAsSb-GaAlAsSb}$  Lattice-Matched Heterojunctions," J. Electrochem. Soc. 121, 416, (1977).
4. Ander, S.J., Scholl, F.W. and Harris, J.S., "AlGaAs Alloys for  $1.0\mu\text{m}-1.8\mu\text{m}$  Heterojunction Devices," Inst. Phys. Conf., Series No. 336, p. 346, Inst. of Phys., Bristol and London, (1977).
5. Pearsal, T., Nahory, R.E. and Pollack, M.A., "Impact Ionization Coefficients for Electrons and Holes in Alloys of  $\text{GaAs}_{1-x}\text{Sb}_x$ ," Paper presented in 1975 Devices Research Conf., Ottawa, Canada, June, 1975.
6. Wood, M.H., Johnson, W.L. and Lampert, M.A., "Use of a Schottky Barrier to Measure Impact Ionization Coefficients in Semiconductors," Solid State Electronics 16, 381, (1973)
7. McIntyre, R.J., "The Distribution of Gains in Uniformity Multiplying Avalanche Photodiodes: Theory," IEEE Trans. of Electron Devices 19, 703, (1972).